

Note: This manuscript was submitted to *Nature* and published in 2022 after peer review:

<https://www.nature.com/articles/s41586-022-04427-4>

## **The lung microbiome regulates brain autoimmunity**

Leon Hosang<sup>1</sup>, Roger Cugota Canals<sup>1</sup>, Felicia Joy van der Flier<sup>1</sup>, Jacqueline Hollensteiner<sup>2</sup>, Rolf Daniel<sup>2</sup>, Alexander Flügel<sup>1\*</sup> & Francesca Odoardi<sup>1,3\*</sup>

Institute for Neuroimmunology and Multiple Sclerosis Research, University Medical Center Göttingen, Germany<sup>1</sup>; Department of Genomic and Applied Microbiology, Göttingen, Germany<sup>2</sup>; Center for Biostructural Imaging of Neurodegeneration, Göttingen, Germany<sup>3</sup>.

\* equal contribution

Correspondence:

Alexander Flügel and Francesca Odoardi  
Institute for Neuroimmunology and Multiple-Sclerosis-Research  
University Medical Center Göttingen  
Von-Siebold-Straße 3a  
37075 Göttingen  
Germany

Phone:       \*\*49-551-39 61158  
FAX:         \*\*49-551-39 61159  
E-mail:      imsf@med.uni-goettingen.de

## **Keywords**

Lung microbiome, autoimmunity, experimental autoimmune encephalomyelitis, multiple sclerosis, central nervous system, T cells.

## **Abbreviations**

APCs: antigen presenting cells, BALF: bronchoalveolar lavage fluid, BBB: blood brain barrier, bSYN: beta-synuclein, CNS: central nervous system, EAE: experimental autoimmune encephalomyelitis, GFP: enhanced green fluorescent protein, i.th.: intrathecal, i.tr.: intratracheal, LPS: lipopolysaccharide, MBP: myelin basic protein, OVA: ovalbumin, p.i.: post immunization, p.o.: per os, p.t.: post transfer, TPLSM: two-photon laser scanning microscopy.

## **Competing financial interests**

The authors declare they have no competing financial interests.

## SUMMARY

**Lung infections and smoking constitute significant risk factors for multiple sclerosis, a T-cell-mediated autoimmune disease of the central nervous system<sup>1</sup>. In addition, the lung serves as a niche for the disease-inducing T cells for long-term survival and for maturation into migration-competent effector T cells<sup>2</sup>. Why the lung tissue in particular plays such an important role in an autoimmune disease of the brain is not yet known. Here we detected a tight interconnection between lung microbiota and the brain's immune reactivity. A dysregulation in the lung microbiome significantly influenced the susceptibility of rats to develop autoimmune central nervous system disease. Shifting the microbiota towards lipopolysaccharide-enriched phyla by local treatment with neomycin induced a type I interferon-primed state in brain-resident microglial cells. Their responsiveness towards autoimmune-dominated type II interferon stimulation was impaired, leading to decreased pro-inflammatory response, immune cell recruitment and clinical signs. Suppressing lipopolysaccharide-producing lung phyla by polymyxin B led to disease aggravation whereas addition of lipopolysaccharide-enriched phyla or lipopolysaccharide recapitulated the neomycin effect. Our data demonstrate the existence of a lung-brain axis where the pulmonary microbiome regulates the immune reactivity of the central nervous tissue and thereby influences its susceptibility to autoimmune disease development.**

## MAIN

Autoimmune processes of the central nervous system (CNS) not only depend on local conditions in the nervous tissue itself, but are also controlled by peripheral organ systems. Of the latter, the lung seems to play an important role. Smoking and lung infections significantly increase the likelihood of multiple sclerosis<sup>1</sup>. In addition, activated T cells, which can trigger an autoimmune reaction within the CNS, migrate into the lung tissue where they develop into migration-competent pathogenic effector cells and survive as long-term memory cells<sup>2</sup>. The lung harbours a specialized milieu characterized by an individual microbial flora. This pulmonary microbiota contributes to the regulation of local immune responses in pathological processes such as asthma, idiopathic pulmonary fibrosis or tumour<sup>3,4</sup>. We here wanted to find out if autoimmune processes of the brain can also be influenced by the lung microbial communities.

We started to investigate if lung microbiota affects the initiation of an autoimmune process inside the lung. For this purpose, we specifically manipulated the microbiota in the lung and established a lung-experimental autoimmune encephalomyelitis model (lung-EAE) (Extended Data Fig. 1a). Daily intratracheal infusion of 1 mg neomycin induced significant changes in lung microbiome diversity and abundance (Fig. 1a) without measurable alterations to the lung-intrinsic cellular immune milieu (Extended Data Fig. 1b-f). Into these pre-treated animals we intravenously transferred myelin basic protein-specific (MBP) T cells and then, 6 hours later, immunized the animals intratracheally with MBP. Intriguingly, after the neomycin treatment the lung-EAE was almost completely blocked. In contrast, rats that did not receive neomycin developed a “classical EAE” (Fig. 1b).

Neomycin applied this way should only act locally in the lung tissue. We wanted to exclude, though, that our observed clinical effects could have been caused by some of the antibiotic drug spilling over from the airways to the gastrointestinal tract and changing the

intestinal microbiota, as the intestinal microbiome can significantly influence immune responses including autoimmune processes of the CNS<sup>5-9</sup>. However, analyses of the gut microbiota after intratracheal neomycin treatment did not show any significant changes in diversity or abundance of the commensal gut bacterial strains (Fig. 1c). Moreover, a direct application of neomycin into the gastrointestinal tract at the dose used for the intratracheal applications induced only minimal changes in the gut microbiome and, importantly, was not sufficient to ameliorate clinical EAE (Extended Data Fig. 2a-b). At 10-fold higher doses of neomycin, changes in the gut's microbiome diversity emerged, but no effects on EAE were observed in this set-up either (Extended Data Fig. 2a-b).

The disease-ameliorating effects of neomycin might theoretically be explained by a direct suppressive effect on the effector T cells rather than by its antibiotic potential. However, even exposure of T cells to 10-fold higher concentrations of neomycin than used in our *in vivo* applications influenced neither their proliferation nor their encephalitogenic potential (Extended Data Fig. 2c-d). Moreover, the presence of the lung microbiota was essential for the neomycin effect, namely application of neomycin in a location lacking a microbial environment, i.e. subcutaneous injection, did not influence EAE, regardless of whether the disease was induced by intratracheal or subcutaneous immunization (Extended Data Fig. 2e-f).

### **T cell function with microbiome dysbiosis**

The data up to this point suggested that dysregulation of the local microbiota can significantly impact on the generation of autoimmune processes in the lung. In order to confirm this, we tracked fluorescently labelled effector T cells (T<sub>MBP</sub> cells)<sup>10</sup> in the course of the lung-EAE model. Unexpectedly, we did not see any effects of local neomycin treatment on the amplification of the T cells within the lung after the intratracheal immunization, nor was there any change in their consequent entry into the blood. However, there was a significant reduction

of T<sub>MBP</sub> cells within the CNS tissue (Fig. 2a). This reduced accumulation of effector T cells within the CNS tissue could not be explained by intrinsic changes in their differentiation or activation state within the lung. Global expression profiles of T<sub>MBP</sub> cells retrieved from neomycin-treated rats and controls revealed that the profound transcriptional changes of T<sub>MBP</sub> cells upon immunization in both treated and control rats were virtually identical (Fig. 2b and Extended Data Fig. 3a-d). Quantitative PCR for genes encoding relevant cytokines, chemokine receptors and factors controlling T cell division, and egression confirmed these data (Fig. 2c and Extended Data Fig. 3e). Neither did we detect any significant changes in numbers or differentiation of the other immune cell populations in the lung (Extended Data Fig. 4a-f).

These data indicate that the disease-suppressing effects of the neomycin-manipulated lung microbiota could not be explained by an influence on the activation process of the T<sub>MBP</sub> cells within the lung tissue. We therefore tested if EAE induced outside of the lung, i.e. by a subcutaneous immunization, could also be influenced by manipulating the lung microbiome. Indeed, this “peripheral EAE” was significantly ameliorated after intratracheal neomycin treatment (Extended Data Fig. 4g). Furthermore, we observed a significant disease-dampening effect when EAE was induced by transfer of effector T cells (transfer EAE), i.e. in a situation in which immunization and a consecutive activation of the T cells *in situ* are not required (Fig. 2d). To confirm the role of the lung microbiota also in this EAE model, we performed a bacterial transfer experiment. We discontinued the intratracheal neomycin treatments of rats and “substituted” the neomycin by daily intratracheal transfers of microbiota isolated from bronchoalveolar lavage fluid (BALF). Importantly, we could observe a significant reduction of the clinical symptoms of transfer EAE in the animals that had received BALF-microbiota from neomycin-treated rats but not in those that had received BALF-microbiota from control rats (Fig. 2e).

In order to determine by which mechanisms the modified lung microbiome interferes with the autoimmune processes we tracked the pathogenic T<sub>MBP</sub> cells in the course of both peripheral and transfer EAE. The T cell numbers and their preclinical migration patterns in the periphery were not affected by the antibiotic treatment. Instead, similarly to neomycin treatment in lung EAE, we found that the numbers of the T<sub>MBP</sub> cells within the CNS tissue were significantly reduced (Fig. 2f-h and Extended Data Fig. 4h).

Notably, the neomycin-induced changes of the lung microbiome did not only influence classical T<sub>MBP</sub>-cell-induced EAE, which preferentially affects the spinal cord white matter. An autoimmune disease of the grey matter of the brain evoked by transfer of beta-synuclein-reactive T cells (T<sub>bSYN</sub> cells)<sup>11</sup> was likewise ameliorated. Also in this set-up, the accumulation of pathogenic T<sub>bSYN</sub> cells in the cortical grey matter of the brain, was reduced in neomycin-treated rats, indicating that changes in the microbiome affect autoimmune responses in the entirety of the CNS tissues (Extended Data Fig. 4i-j).

These data suggest that the manipulation of the lung microbiome does not affect the T cell-triggered autoimmune process in the periphery but rather at the border of or within the CNS. We therefore next explored the interaction of the effector T cells with the endothelium of the blood-brain barrier (BBB). T<sub>MBP</sub> cells enter the CNS tissue from leptomeningeal vessels of the spinal cord where they crawl on the endothelial surface using integrins and chemokines as adhesion factors<sup>12,13</sup>. Neomycin treatment did not change the expression of these relevant adhesion molecules in T<sub>MBP</sub> cells, either in active or transfer EAE (Extended Data Fig. 5a-b). Moreover, intravital two-photon laser scanning microscopy (TPLSM) revealed that T<sub>MBP</sub> cells displayed the typical migratory pattern within leptomeningeal vessels (Extended Data Fig. 5c, Supplementary Video 1). To exclude any effects on the endothelium due to the different inflammatory conditions of the CNS in neomycin-treated vs control animals, we tracked brain-

antigen-ignorant T<sub>OVA</sub> cells. These cells also crawl within leptomeningeal vessels and transgress into the leptomeningeal milieu – though to a lesser extent than T<sub>MBP</sub> cells<sup>12,14</sup>. Of note, the intra- and extra-vascular locomotion behaviour and diapedesis of the T<sub>OVA</sub> cells were virtually identical after neomycin treatment (Extended Data Fig. 5d-e, Supplementary Video 2). Furthermore, the expression profiles from endothelial cells of neomycin-treated and control animals did not show significant regulation of genes that determine the barrier function or the adhesiveness of the vasculature (Extended Data Fig. 5f) and TPLSM did not provide any evidence for a leaky BBB (Extended Data Fig. 5g), indicating that the changes to the lung microbiome by neomycin did not influence the properties of the CNS endothelium.

### **Lung microbiota influences microglia**

We next examined if the initiation of the autoimmune process within the CNS tissue was changed after the neomycin treatment. Upon endothelial transmigration, T<sub>MBP</sub> cells become reactivated within the CNS upon re-encounter of their cognate antigen presented by local antigen presenting cells (APCs)<sup>14</sup>. The consecutive T cellular release of cytokines – a classical type II interferon (IFN) dominated profile – stimulate resident immune-competent cells and thereby trigger the recruitment of peripheral immune cells which induce structural damage and clinical signs<sup>11,15-18</sup>. Longitudinal analyses in the course of EAE indeed revealed a significantly decreased inflammatory milieu in the CNS tissue of neomycin-treated rats (Fig. 3a and Extended Data Fig. 6a). This dampened autoimmune inflammation could not be explained by a failure of the T<sub>MBP</sub> cells to become reactivated within the CNS tissue (Extended Data Fig. 6b-c). Neither could we find significant differences in the differentiation, relative numbers, or cytokine expression of recruited immune cells (Extended Data Fig. 6). Since the full manifestation of clinical signs occurs only after a secondary glial inflammatory response, we speculated that the transmission of the T-cellular immune trigger within the tissue might be

disturbed. Therefore, we next tested the functionality of microglia, the CNS-resident immune cell population able to react very sensitively to T cell-derived stimuli<sup>19</sup>, e.g. by producing pro-inflammatory factors, chemokines and up-regulate expression of MHC-II molecules<sup>20</sup>. We indeed found that microglia in acute autoimmune lesions did not assume their characteristic activatory morphological transformation (Extended Data Fig. 7a). Furthermore, in contrast to the recruited myeloid cells, microglia displayed a reduced expression of CXCL9, CXCL10, CXCL11, iNOS and MHCII (Fig. 3b and Extended Data Fig. 6d). The relevance of microglia in EAE pathogenesis and lung microbiome regulation was further supported by treating the rats with minocycline, which interferes with the activation of microglia<sup>21</sup>. We in fact observed a significant suppression of transfer EAE upon minocycline application (Fig. 3c). Importantly, neomycin pre-treatment of the rats did not add to the disease-dampening effect of minocycline (Fig. 3c). Very similar results were obtained when targeting microglia by an ablation strategy using a selective colony stimulating factor 1 receptor (CSF1R) inhibitor<sup>22</sup> (Extended Data Fig. 7b-c). Although we cannot rule out that changes in the peripheral or recruited immune cells could contribute to the clinical effects, our data indicate that it is mainly the microglia that are influenced after the neomycin-induced lung microbiome dysbiosis and that mediate the altered autoimmune response.

Interestingly, even in the absence of autoimmune inflammation we noted a significant change in the microglial morphology after intratracheal neomycin treatment, both in spinal cord and brain cortical grey matter tissue. The lengths and numbers of their branches were significantly reduced whereas the numbers of microglia were unchanged (Fig. 4a, Extended Data Fig. 7d-f, Supplementary Video 3). Global transcriptome analyses of microglia demonstrated significant transcriptional changes, though in a restricted number of genes. Thereby, genes such as *Mx1*, *Mx2*, *Rsad2*, *Oas1a* and *Irf7* were upregulated whereas *Il6st* and

*Irf8* were downregulated (Fig. 4b and Suppl. Table 1). GO term analysis revealed that the majority of the upregulated genes could be attributed to the type I IFN signalling pathway (Extended Data Fig. 7g). The regulations of several of these genes were confirmed with quantitative PCR (Fig. 4c and Extended Data Fig. 7h). Remarkably, the genes which were changed in total tissue and microglia overlapped to a large extent, indicating that lung microbiota-induced changes of the CNS tissue affect primarily microglia (Fig. 4b and Extended Data Fig. 7i). Indeed, astrocytes, the other major immune-competent glial cell population of the CNS, did not show this shift towards a type I IFN signalling pathway (Extended Data Fig. 7j).

It should be noted that a shift of microglial reactivity to a type I IFN immune reactivity can modulate microglial responsiveness towards the type II IFN-dominated autoimmune challenge<sup>23</sup>. This could explain the observed diminished tissue inflammation (Fig. 3a and Extended Data Fig. 6a). Accordingly, intrathecal (i.th.) injection of poly I:C, which evokes a type I IFN signature via toll-like receptor 3 signalling<sup>24</sup>, significantly interfered with the EAE induction (Fig. 4d). The changed reactivity of the microglia also became evident after a direct i.th. stimulation with IFN $\gamma$  and TNF $\alpha$ . In fact, microglial cells from rats pre-treated with neomycin showed a reduced activation after the local challenge with these pro-inflammatory cytokines. Furthermore, a significantly reduced recruitment of inflammatory cells could be observed (Extended Data Fig. 8a). Analyses of *in vitro*-stimulated microglia isolated from neomycin pre-treated or control rats confirmed a reduced reactivity of the microglia upon IFN $\gamma$  stimulation (Extended Data Fig. 8b).

### **LPS as lung microbial CNS regulator**

In order to find out how these alterations in microglial reactivity are linked to the lung microbiome we next focussed on the changes of the lung commensal bacterial communities upon intratracheal neomycin treatment. Gram-negative Bacteroidetes were the most abundant

bacteria phylum (37%) with a 2.5 fold increase compared to the PBS-treated group (Fig. 5a). In this phylum, the most increased families were affiliated to Prevotellaceae, Muribaculaceae and Rikenellaceae, all of which are anaerobes and comprise members resistant to neomycin (Fig. 5b). We also observed an upregulation in other bacterial families, including Lachnospiraceae and Lactobacillus. These qualitative changes in lung microbiota composition were associated with a significant increase in the total bacteria load (Fig. 1a).

We next wanted to find out if Bacteroidetes – the phylum mostly affected by the neomycin treatment – would be relevant for the observed clinical effects. Therefore, we transferred an inactivated strain of the Bacteroidetes phylum, *Prevotella melaninogenica*. In fact, the intratracheal transfer of *Prevotella melaninogenica* led to significantly dampened clinical EAE (Fig. 5c). Transfer of the microbiota by gastrointestinal gavage did not change the disease, which provides further support for the relevance of the lung microbiome in the regulation of the CNS immune reactivity (Extended Data Fig. 8c). The efficiency of the metabolically inactive *Prevotella melaninogenica* hints at a structural microbial component, which mediates the immune modulating effects within the CNS. One potential candidate for this is the bacterial cell wall component lipopolysaccharide (LPS), which is well known to evoke type I IFN responses<sup>25,26</sup>. Considering that Bacteroidetes contribute up to 80 % of LPS production in the gut<sup>27</sup>, we next quantified the LPS concentration within the BALF. Indeed, we observed a significant LPS increase in neomycin-treated rats (Extended Data Fig. 8d). This elevated intrapulmonary LPS levels correlated with an increased type I IFN signature in interstitial macrophages and neutrophils in the lung (Extended Data Fig. 8e). Interestingly, intratracheal treatment with the antibiotic drug vancomycin, which did not induce a shift towards LPS-producing phyla (Extended Data Fig. 8d and Extended Data Fig. 9a-b), did not change the microglial expression profile and was not effective in ameliorating EAE (Extended Data Fig. 9c-g). Furthermore, intratracheal application of the LPS-neutralizing antibiotic

peptide polymyxin B<sup>28,29</sup> significantly increased EAE severity (Extended Data Fig. 10a). In order to directly test the role of LPS we increased its local levels by intratracheal application of LPS from *Escherichia coli* or *Prevotella melaninogenica*. As was the case with the neomycin treatment or microbiota transfer, the LPS supplementation in the lung led to an amelioration of EAE (Fig. 5d and Extended Data Fig. 10b). LPS has been reported to penetrate the BBB and to evoke functional changes in microglia<sup>30,31</sup>. Therefore, we finally applied LPS directly into the CNS. Intrathecal injection of LPS evoked clear disease dampening effects even exceeding those observed after intratracheal LPS applications (Fig. 5e and Extended Data Fig. 9c). The data therefore support the view that a shift towards LPS-producing phyla induces a type I IFN response in the CNS, which can serve as underlying mechanism for the resistance against autoimmune processes (Extended Data Fig. 9d).

Our study indicates a new and unexpected functional connection between lung and brain. This connection is controlled by the local lung microbiota, which apparently continuously sends signals to the microglia, the brain's "immune cells"<sup>19</sup>. The microglial cells adapt their immunological responsiveness according to these microbial signals. The lung is the most extended body surface<sup>32</sup> in contact with the outside environment and it is therefore constantly exposed to microbes and contaminants. These pathogens can also pose a danger to the CNS. The pulmonary microbiome, which is directly located at the interface with the outside environment and which in its nature is trimmed to react to these external threats, can therefore act as a kind of remote warning system for the sensitive CNS.

Up until now the gut microbiome has had the main focus of attention as regulator of CNS immune functions<sup>33</sup>. There are, however, clear differences in the location and the nature of the microbial signals that are responsible for this regulation. Although remote effects of the gut microbiome on the CNS have been postulated<sup>8,34,35</sup>, the major focus is on effects in the

intestinal milieu, immune structures in the intestine and the draining lymph nodes. Microbial antigens that resemble those of CNS structures could play a role as the initial trigger of the pathogenic T cell response<sup>9</sup>. Conversely, a regulatory function of microbial factors, e.g. the polysaccharide A is discussed<sup>36</sup>. Furthermore, microbial nutrients or their derivatives such as short-chained fatty acids or tryptophan metabolites can influence the activation and differentiation of pathogenic T cells<sup>37,38</sup>. Although a contribution by microbial metabolites cannot be ruled out in the effects on CNS autoimmunity observed here, our data favor LPS as trigger of a type I IFN response which interferes with the autoimmune process in EAE models and multiple sclerosis<sup>23,39,40</sup>. Perhaps the most prominent difference between the gut and lung microbiome is the extent of manipulation necessary to change the immunological situation. Influencing CNS autoimmunity via the gut requires drastic interference with the gut microbiome, for example a high-dosed combined antibiotics that almost completely depletes the microbiota, or housing the animals in a sterile environment. The effects of such interference are by nature strong and extend from an atrophy of secondary immune organs to massive local problems, e.g. the development of a megacolon<sup>34,41-43</sup>. In the lung, in contrast, only minimum manipulations – here only a moderate shift in the bacterial diversity – is enough to achieve a corresponding microglial reaction. The pulmonary microbiome is distinct and comprises only a quantitatively tiny population in comparison to that of the gut (at least  $10^8$  in magnitude)<sup>44</sup>. Therefore, minimal outside influences may suffice to unbalance it. Furthermore, the particularities of the blood-air barrier and the special integration of the lung in the circulatory system can come into play. Thus, the distance to be conquered by microbial signal substances to reach the blood most likely is much shorter for the pulmonary commensals than for the gut's intestinal commensals. Especially in the alveolar area, this distance for the purpose of optimized oxygen exchange is minimized: the border of the cell layers of alveolar cells and capillary endothelium consists only of a shared basement membrane. Moreover, the direct blood flow

out of the lung into the arterial system provides an unfiltered access to the CNS. The gut has the liver as “firewall” between itself and the CNS<sup>45</sup>.

In conclusion, we here demonstrate that a well-balanced equilibrium of the pulmonary microbiota tunes the activation state of microglia, most likely via incremented colonization of LPS-producing bacterial taxa. This observation could be of importance in a clinical perspective: infections of the lung, smoking, therapeutic manipulations and environmental factors all can act on the pulmonary microbiome and thus might influence the brain’s immune reactivity. This tight interconnection could potentially be therapeutically exploited, e.g. by local application of probiotics or certain antibiotics. A targeted manipulation of the CNS immune reactivity is certainly not only an interesting treatment option for an autoimmune situation, but in addition for a wide range of CNS diseases where the reactivity of the brain’s innate immune response is involved, e.g. in infectious or degenerative disorders.

## REFERENCES

- 1 Olsson, T., Barcellos, L. F. & Alfredsson, L. Interactions between genetic, lifestyle and environmental risk factors for multiple sclerosis. *Nat Rev Neurol* **13**, 25-36, doi:10.1038/nrneurol.2016.187 (2017).
- 2 Odoardi, F. *et al.* T cells become licensed in the lung to enter the central nervous system. *Nature* **488**, 675-679 (2012).
- 3 O'Dwyer, D. N., Dickson, R. P. & Moore, B. B. The lung microbiome, immunity, and the pathogenesis of chronic lung disease. *J Immunol* **196**, 4839-4847, doi:10.4049/jimmunol.1600279 (2016).
- 4 Jin, C. *et al.* Commensal Microbiota Promote Lung Cancer Development via  $\gamma\delta$  T Cells. *Cell* **176**, 998-1013.e1016, doi:10.1016/j.cell.2018.12.040 (2019).
- 5 Yokote, H. *et al.* NKT cell-dependent amelioration of a mouse model of multiple sclerosis by altering gut flora. *Am J Pathol* **173**, 1714-1723, doi:10.2353/ajpath.2008.080622 (2008).
- 6 Ochoa-Repáraz, J. *et al.* Role of gut commensal microflora in the development of experimental autoimmune encephalomyelitis. *J Immunol* **183**, 6041-6050, doi:10.4049/jimmunol.0900747 (2009).
- 7 Berer, K. *et al.* Commensal microbiota and myelin autoantigen cooperate to trigger autoimmune demyelination. *Nature* **479**, 538-541 (2011).
- 8 Rothhammer, V. *et al.* Type I interferons and microbial metabolites of tryptophan modulate astrocyte activity and central nervous system inflammation via the aryl hydrocarbon receptor. *Nat.Med.* **22**, 586-597 (2016).
- 9 Miyauchi, E. *et al.* Gut microorganisms act together to exacerbate inflammation in spinal cords. *Nature* **585**, 102-106, doi:10.1038/s41586-020-2634-9 (2020).

- 10 Flügel, A., Willem, M., Berkowicz, T. & Wekerle, H. Gene transfer into CD4<sup>+</sup> T lymphocytes: green fluorescent protein-engineered, encephalitogenic T cells illuminate brain autoimmune responses. *Nat.Med.* **5**, 843-847 (1999).
- 11 Lodygin, D. *et al.*  $\beta$ -Synuclein-reactive T cells induce autoimmune CNS grey matter degeneration. *Nature* **566**, 503-508 (2019).
- 12 Bartholomäus, I. *et al.* Effector T cell interactions with meningeal vascular structures in nascent autoimmune CNS lesions. *Nature* **462**, 94-98 (2009).
- 13 Kivisäkk, P. *et al.* Localizing central nervous system immune surveillance: meningeal antigen-presenting cells activate T cells during experimental autoimmune encephalomyelitis. *Ann.Neurol* **65**, 457-469 (2009).
- 14 Lodygin, D. *et al.* A combination of fluorescent NFAT and H2B sensors uncovers dynamics of T cell activation in real time during CNS autoimmunity. *Nat.Med.* **19**, 784-790 (2013).
- 15 Starossom, S. C. *et al.* Galectin-1 deactivates classically activated microglia and protects from inflammation-induced neurodegeneration. *Immunity* **37**, 249-263, doi:10.1016/j.immuni.2012.05.023 (2012).
- 16 Kawakami, N. *et al.* The activation status of neuroantigen-specific T cells in the target organ determines the clinical outcome of autoimmune encephalomyelitis. *J.Exp.Med.* **199**, 185-197 (2004).
- 17 Odoardi, F. *et al.* Instant effect of soluble antigen on effector T cells in peripheral immune organs during immunotherapy of autoimmune encephalomyelitis. *Proc.Natl.Acad.Sci.U.S.A* **104**, 920-925 (2007).
- 18 Heppner, F. L. *et al.* Experimental autoimmune encephalomyelitis repressed by microglial paralysis. *Nat.Med.* **11**, 146-152 (2005).
- 19 Hanisch, U. K. & Kettenmann, H. Microglia: active sensor and versatile effector cells in the normal and pathologic brain. *Nat Neurosci* **10**, 1387-1394, doi:10.1038/nn1997 (2007).
- 20 Rock, R. B. *et al.* Transcriptional response of human microglial cells to interferon-gamma. *Genes Immun* **6**, 712-719, doi:10.1038/sj.gene.6364246 (2005).
- 21 Popovic, N. *et al.* Inhibition of autoimmune encephalomyelitis by a tetracycline. *Ann Neurol* **51**, 215-223, doi:10.1002/ana.10092 (2002).
- 22 Elmore, M. R. *et al.* Colony-stimulating factor 1 receptor signaling is necessary for microglia viability, unmasking a microglia progenitor cell in the adult brain. *Neuron* **82**, 380-397, doi:10.1016/j.neuron.2014.02.040 (2014).
- 23 Prinz, M. *et al.* Distinct and nonredundant in vivo functions of IFNAR on myeloid cells limit autoimmunity in the central nervous system. *Immunity* **28**, 675-686, doi:10.1016/j.immuni.2008.03.011 (2008).
- 24 Khoroshi, R. *et al.* Induction of endogenous Type I interferon within the central nervous system plays a protective role in experimental autoimmune encephalomyelitis. *Acta Neuropathol* **130**, 107-118, doi:10.1007/s00401-015-1418-z (2015).
- 25 McNab, F., Mayer-Barber, K., Sher, A., Wack, A. & O'Garra, A. Type I interferons in infectious disease. *Nat Rev Immunol* **15**, 87-103, doi:10.1038/nri3787 (2015).
- 26 Bradley, K. C. *et al.* Microbiota-driven tonic interferon signals in lung stromal cells protect from influenza virus infection. *Cell Rep* **28**, 245-256.e244, doi:10.1016/j.celrep.2019.05.105 (2019).
- 27 d'Hennezel, E., Abubucker, S., Murphy, L. O. & Cullen, T. W. Total lipopolysaccharide from the human gut microbiome silences toll-like receptor signaling. *mSystems* **2**, doi:10.1128/mSystems.00046-17 (2017).
- 28 Yang, D. *et al.* Dysregulated lung commensal bacteria drive interleukin-17B production to promote pulmonary fibrosis through their outer membrane vesicles. *Immunity* **50**, 692-706.e697, doi:10.1016/j.immuni.2019.02.001 (2019).
- 29 Bhor, V. M., Thomas, C. J., Surolia, N. & Surolia, A. Polymyxin B: an ode to an old antidote for endotoxic shock. *Mol Biosyst* **1**, 213-222, doi:10.1039/b500756a (2005).
- 30 Vargas-Caraveo, A. *et al.* Lipopolysaccharide enters the rat brain by a lipoprotein-mediated transport mechanism in physiological conditions. *Sci Rep* **7**, 13113, doi:10.1038/s41598-017-13302-6 (2017).
- 31 Sandiego, C. M. *et al.* Imaging robust microglial activation after lipopolysaccharide administration in humans with PET. *Proc Natl Acad Sci U S A* **112**, 12468-12473, doi:10.1073/pnas.1511003112 (2015).

- 32 Dickson, R. P., Erb-Downward, J. R., Martinez, F. J. & Huffnagle, G. B. The microbiome and the respiratory tract. *Annu Rev Physiol* **78**, 481-504, doi:10.1146/annurev-physiol-021115-105238 (2016).
- 33 Belkaid, Y. & Hand, T. W. Role of the microbiota in immunity and inflammation. *Cell* **157**, 121-141 (2014).
- 34 Erny, D. *et al.* Host microbiota constantly control maturation and function of microglia in the CNS. *Nat. Neurosci.* **18**, 965-977 (2015).
- 35 Braniste, V. *et al.* The gut microbiota influences blood-brain barrier permeability in mice. *Sci. Transl. Med.* **6**, 263ra158 (2014).
- 36 Wang, Y. *et al.* An intestinal commensal symbiosis factor controls neuroinflammation via TLR2-mediated CD39 signalling. *Nat. Commun.* **5**, 4432 (2014).
- 37 Luu, M. *et al.* The short-chain fatty acid pentanoate suppresses autoimmunity by modulating the metabolic-epigenetic crosstalk in lymphocytes. *Nat Commun* **10**, 760, doi:10.1038/s41467-019-08711-2 (2019).
- 38 Sonner, J. K. *et al.* Dietary tryptophan links encephalogenicity of autoreactive T cells with gut microbial ecology. *Nat Commun* **10**, 4877, doi:10.1038/s41467-019-12776-4 (2019).
- 39 Jakimovski, D., Kolb, C., Ramanathan, M., Zivadinov, R. & Weinstock-Guttman, B. Interferon  $\beta$  for multiple sclerosis. *Cold Spring Harb Perspect Med* **8**, doi:10.1101/cshperspect.a032003 (2018).
- 40 Guo, B., Chang, E. Y. & Cheng, G. The type I IFN induction pathway constrains Th17-mediated autoimmune inflammation in mice. *J Clin Invest* **118**, 1680-1690, doi:10.1172/jci33342 (2008).
- 41 Bauer, H., Horowitz, R. E., Levenson, S. M. & Popper, H. The response of the lymphatic tissue to the microbial flora. Studies on germfree mice. *Am J Pathol* **42**, 471-483 (1963).
- 42 Smith, K., McCoy, K. D. & Macpherson, A. J. Use of axenic animals in studying the adaptation of mammals to their commensal intestinal microbiota. *Semin Immunol* **19**, 59-69, doi:10.1016/j.smim.2006.10.002 (2007).
- 43 Kennedy, E. A., King, K. Y. & Baldrige, M. T. Mouse microbiota models: comparing germ-free mice and antibiotics treatment as tools for modifying gut bacteria. *Front Physiol* **9**, 1534, doi:10.3389/fphys.2018.01534 (2018).
- 44 Wypych, T. P., Wickramasinghe, L. C. & Marsland, B. J. The influence of the microbiome on respiratory health. *Nat Immunol* **20**, 1279-1290, doi:10.1038/s41590-019-0451-9 (2019).
- 45 Balmer, M. L. *et al.* The liver may act as a firewall mediating mutualism between the host and its gut commensal microbiota. *Sci Transl Med* **6**, 237ra266, doi:10.1126/scitranslmed.3008618 (2014).

## DATA AVAILABILITY

RNA-seq data sets have been deposited online in the Gene Expression Omnibus (GEO database) and BioProject with accession codes GSE191287, GSE192411 and PRJNA789820.

Source data are provided with this paper.

## ACKNOWLEDGEMENTS

The authors thank S. Schwarz for helping in the quantification of the *Tuf* genes, M. Ulisse for contributing to characterizing the lung immune milieu, G. Salinas for performing the transcriptome analyses, O. Shomroni for the analysis of the transcriptome data, S. Hamann and

M. Weig and M. Heinemann for technical assistance, A. Poehlein for performing the 16S rRNA sequencing, D. Schneider for providing the bioinformatic amplicon processing pipeline and D. Miljković for helping with animal experiments and carefully reading the manuscript. We are grateful to C. Ludwig for text editing. This work was supported by the Deutsche Forschungsgemeinschaft (DFG, German Research Foundation) RK-Grant FL 377/3-1; FL 377/2-2; SFB 1328/1 project A01, project No. 335447717; OD 87/1-1, OD 87/3-1; SFB TRR 274/1 2020 projects A03 + A04, project No. 408885537; and by the European Commission under The European Union's Horizon 2020 research and innovation programme, grant agreement No. 101021345 (T-Neuron). LH is supported by the Klaus Faber Stiftung.

## AUTHOR CONTRIBUTIONS

L.H. performed most experimental work and together with A.F. and F.O. wrote the paper. R.C.C. contributed with immune cell characterizations by qPCR analyses and flow cytometry and by performing EAE experiments. F.J.v.d.F. performed the intravital TPLSM and supported L.H. with inducing and analysing autoimmune models. J.H. contributed with the microbiome analyses, R.D. with his expertise in microbiome biology. A.F. together with F.O. designed the study, coordinated the experimental work and wrote the manuscript with inputs from co-authors.

## LEGENDS

**Fig. 1: Manipulations of the lung microbiota affect CNS autoimmunity.** a, i.tr. neomycin (NEO) treatment induces lung microbiota dysbiosis. Left: Principal component analysis (PCA) of microbiota composition of BALF from animals i.tr. treated with PBS or NEO at the indicated concentration for 7 days. 16S rRNA sequencing. Middle: Corresponding Shannon and phylogenetic diversity indices. Right: Quantification of bacterial abundance based on *tuf*-gene

expression via 16S rRNA based quantitative PCR. Mean  $\pm$  SEM. Cumulative data of 2 independent experiments. n=6 (PBS, 0.1 and 1mg NEO). **b**, i.tr. NEO treatment ameliorates active EAE. Lung EAE was induced in rats pre-treated i.tr. with NEO or PBS for 7 days. Clinical parameters: Body weight change (lines) and clinical scores (bars) over the EAE course, incidence (%), average onset (days p.i.), average peak score, average cumulative score. Mean  $\pm$  SEM. Representative data of 4 independent experiments. n=6 (PBS), n=9 (NEO). **c**, i.tr. NEO treatment does not induce gut microbiota dysbiosis. PCA, Shannon and phylogenetic diversity indices and quantification of bacterial abundance in fecal samples from the same animals as in **a**. Mean  $\pm$  SEM. n=4 (PBS), n=5 (0.1 and 1mg NEO). **a**, **c**, Statistical significance determined via one-way ANOVA with Tukey's multiple comparisons test in the case of Gaussian distribution and Kruskal-Wallis test with Dunn's multiple comparisons test in the case of non-Gaussian distribution. **b**, Statistical significance determined via unpaired two-tailed *t*-test in the case of Gaussian distribution and Mann-Whitney test in the case of non-Gaussian distribution. \* $P < 0.05$ , \*\*\* $P < 0.001$ .

**Fig. 2. Lung dysbiosis does not influence T cell activation and migration.** **a-c**, Lung EAE was induced in rats i.tr. pre-treated for 7 days with NEO or PBS. **a**, NEO treatment reduces CNS invasion but not the peripheral T cell distribution. T<sub>MBP</sub> cell number. Flow cytometry. D7 p.i. Mean  $\pm$  SEM. Cumulative data from 2 independent experiments. n=9 (PBS), n=5 (NEO). **b-c**, i.tr. NEO treatment does not change the T cellular transcriptome. **b**, Differential gene expression of T<sub>MBP</sub> cells from lungs on D1 p.i. in PBS vs NEO pre-treated animals. **c**, Cytokine expression of T<sub>MBP</sub> cells in lungs of animals immunized with (+MBP, n=8/group) or without MBP (-MBP, n=3/group). D1 p.i. Quantitative PCR. Mean  $\pm$  SEM. Cumulative data of 2 independent experiments. **d**, i.tr. NEO treatment ameliorates transfer EAE. Clinical parameters. Mean  $\pm$  SEM. Cumulative data of 3 independent experiments. n=9 (PBS), n=11 (NEO). **e**, Lung

microbiota of NEO-treated animals ameliorate EAE. Animals were i.tr. pre-treated with NEO. The treatment was interrupted before T<sub>MBP</sub> cell transfer and continued via i.tr. transfer of microbiota isolated from BALF of animals i.tr. pre-treated with NEO or PBS. Clinical parameters. Mean ± SEM. Cumulative data of 2 independent experiments. n=6 (PBS, NEO). **f-h**, NEO pre-treatment reduces T<sub>MBP</sub> cell entry into the spinal cord. **f**, T<sub>MBP</sub> cell number. D7 p.t. Mean ± SEM. Representative data of 3 independent experiments. n=4 (PBS), n=5 (NEO). **g**, Kinetics of T<sub>MBP</sub> cell invasion. Flow cytometry. Mean ± SEM. Representative data of 2 independent experiments. n=4-6/time point (PBS), n=4-7/time point (NEO). **h**, CNS-invasion of T<sub>MBP</sub> cells (green). Intravital TPLSM. Representative images of 2 independent experiments. Red: Vessels. **a, c-g**, Statistical significance determined via unpaired two-tailed *t*-test in the case of Gaussian distribution and Mann-Whitney test in the case of non-Gaussian distribution. \**P* < 0.05, \*\**P* < 0.01, \*\*\**P* < 0.001.

**Fig. 3. Lung dysbiosis affects microglia immune reactivity.** **a-b**, EAE was induced in rats pre-treated i.tr. with NEO or PBS by transfer of T<sub>MBP</sub> cells. **a**, i.tr. NEO treatment reduces T<sub>MBP</sub> cell-mediated CNS inflammation. Number of endogenous αβTCR<sup>+</sup> CD4<sup>+</sup> and CD8<sup>+</sup> T cells, CD45RA<sup>+</sup> B cells and CD45<sup>high</sup> CD11b<sup>+</sup> MΦ (recruited monocytes and resident macrophages) isolated from the spinal cord at the indicated time points after transfer. Flow cytometry. Mean ± SEM. Representative data of 3 independent experiments. n=4/time point (PBS), n=4-6/time point (NEO). **b**, i.tr. NEO treatment dampens microglial response to a T cell-mediated attack. Differential expression of iNOS (*Nos2*), MHC-II (*Rt1ba*) and chemokines in microglia sorted at the initiation stage of the EAE from PBS- or NEO-treated animals. Quantitative PCR. Mean ± SEM. Representative data of 2 independent experiments. n=4/condition (PBS), n=3/condition (NEO). **c**, Minocycline ameliorates EAE but does not add to the disease-ameliorating effects of i.tr. NEO treatment. Animals were treated i.p. with minocycline/vehicle and i.tr. with

NEO/PBS. After 7 days, EAE was induced by T<sub>MBP</sub> cell transfer. The treatments were continued throughout the entire disease course. Clinical parameters. Mean ± SEM. Cumulative data of 2 independent experiments. n=7 (Vehicle/PBS, Minocycline/PBS, Minocycline/NEO), n=6 (Vehicle/NEO). a-b, Statistical significance determined via unpaired two-tailed *t*-test in the case of Gaussian distribution and Mann-Whitney test in the case of non-Gaussian distribution. c, Statistical significance determined via one-way ANOVA with Tukey's multiple comparisons test. \**P* < 0.05, \*\**P* < 0.01, \*\*\**P* < 0.001, ns: not-significant.

**Fig. 4. Lung dysbiosis shifts microglia to a type I IFN signature.** **a**, i.tr. NEO treatment induces an altered microglia morphology. Confocal-3D reconstructions of Iba1<sup>+</sup> microglia in the grey matter of the spinal cord 7 days after i.tr. PBS or NEO treatment. Representative images of 16 different cells from 3 animals/group. **b-c**, i.tr. NEO treatment induces a type I IFN signature in spinal cord microglia. **b**, Comparison of global gene expression profile in CD45<sup>low</sup> CD11b<sup>+</sup> microglia sorted from the spinal cord of animals treated with PBS or NEO for 7 days. Candidate genes upregulated in NEO vs PBS treated animals are indicated as red dots. Genes significantly up- or downregulated (*P* < 0.05) but below the 0.5 fold change cut-off are indicated as light red and light blue dots, respectively. Type I IFN-regulated genes are indicated. Bold: Genes confirmed via quantitative PCR. **c**, Set-up as in b. Expression of type I IFN-regulated genes measured by quantitative PCR. Mean ± SEM. Cumulative data of 3 independent experiments. n=5-12/condition (PBS), n=5-12/condition (NEO). **d**, Intrathecal poly I:C treatment ameliorates EAE. EAE was induced by transfer of T<sub>MBP</sub> cells. Poly I:C was administered intrathecally on day 0, 2 and 4 after T<sub>MBP</sub> cell transfer. Clinical parameters. Mean ± SEM. Cumulative data of 2 independent experiments. n=6 (PBS, NEO). c-d, Statistical significance determined via unpaired two-tailed *t*-test in the case of Gaussian distribution and

Mann-Whitney test in the case of non-Gaussian distribution. \* $P < 0.05$ , \*\* $P < 0.01$ , \*\*\* $P < 0.001$ .

**Fig. 5. Pulmonary LPS controls CNS autoimmunity. a-b**, Neomycin induces a shift towards LPS producing phyla in the lung microbiota. **a**, Average relative abundance of bacterial phyla of lung microbiota in PBS- or NEO-treated animals. **b**, Corresponding heat map depicting the relative abundance of lung bacterial inhabitants at family level. **c**, i.tr. administration of inactivated *Prevotella melaninogenica* has an EAE suppressive effect. EAE was induced by transfer of  $T_{MBP}$  cells. Clinical parameters upon daily i.tr. treatment started 7 days before  $T_{MBP}$  cell transfer and continued throughout the entire disease course. Mean  $\pm$  SEM. Cumulative data of 2 independent experiments.  $n=6$  (PBS),  $n=8$  (*Prevotella melaninogenica*). **d**, i.tr. treatment with LPS from *Prevotella melaninogenica* ameliorates EAE. Transfer EAE was induced in animals pre-treated i.tr. for 7 days with PBS or LPS at the indicated concentration. The treatment was continued throughout the entire disease course. Clinical parameters. Mean  $\pm$  SEM. Cumulative data of 2 independent experiments.  $n=9$  (PBS),  $n=6$  (0.01mg LPS),  $n=7$  (0.025mg LPS). **e**, Intrathecal administration of LPS from *Prevotella melaninogenica* has a disease suppressive effect. LPS (0.005 mg/rat) was administered on day 0, 2 and 4 after  $T_{MBP}$  cell transfer. Clinical parameters. Mean  $\pm$  SEM. Cumulative data of 2 independent experiments.  $n=7$  (PBS),  $n=6$  (LPS). **c, e**, Statistical significance determined via unpaired two-tailed  $t$ -test in the case of Gaussian distribution and Mann-Whitney test in the case of non-Gaussian distribution. **d**, Statistical significance determined via one-way ANOVA with Tukey's multiple comparisons test. \* $P < 0.05$ , \*\* $P < 0.01$ , \*\*\* $P < 0.001$ .

## METHODS

## **Animals**

Male and female 6 – 10 weeks old wild type (wt) and bSYN TCR-transgenic rats<sup>11</sup> on a LEW/Crl (*Rattus norvegicus*) background were used for all experiments and for the generation of T cell lines. The animals were kept in GR9000 IVC cages at a 12/12 h light/dark cycle with food and water provided *ad libitum*. They were bred and raised at the animal facilities of the University Medical Center Göttingen. All experiments were performed in accordance with the regulations of animal welfare of Lower Saxony, Germany. No differences were noted between the sexes.

## **Antigens**

Myelin basic protein (MBP) was extracted from guinea pig brain as previously described<sup>46</sup>,  $\beta$ -Synuclein<sub>93-111</sub> peptide (bSYN) was synthesized by the peptide facility of the Charité (Berlin), and Ovalbumin (OVA) was purchased from Sigma-Aldrich.

## **Generation and culturing of T cells**

CD4<sup>+</sup> T cells retrovirally transduced to express Life-act Turquoise (CFP) or eGFP (GFP) and reactive against MBP (T<sub>MBP</sub>), bSYN (T<sub>bSYN</sub>) or OVA (T<sub>OVA</sub>) were generated as previously reported<sup>10,11</sup>. Briefly, female Lewis rats were immunized subcutaneously at the tail base (s.c.) with 150  $\mu$ L of an emulsion consisting to equal parts of antigen (MBP, bSYN or OVA; 1 mg/mL) and complete Freund's adjuvant (CFA, Difco) containing *Mycobacterium tuberculosis H37Ra* extract (2 mg/mL, BD). 9 – 10 days after immunization, the cell suspension obtained from the draining lymph nodes was co-cultured with GP+E86 packaging cell lines producing replication-deficient retroviruses expressing a fluorescent protein of interest and an antibiotic resistant gene in the presence of MBP (10  $\mu$ g/mL), OVA (10  $\mu$ g/ml) or bSYN (8  $\mu$ g/mL) in DMEM based-medium containing 1 % rat serum. 48 h later, T cells were expanded by adding DMEM-based medium containing horse serum (10 %, Biochrom AG) and murine IL2. Starting from D4 after antigen stimulation, transduced T cells were selected by the addition of G418

(400 mg/mL, Thermo Fisher) for two weeks or puromycin (1 µg/mL, Carl Roth) for one week. On D7 after primary stimulation,  $3.5 \times 10^6$  T cells were challenged with the cognate antigen in the presence of  $70 \times 10^6$  irradiated thymic APCs. The primary cell lines underwent at least 3 cycles of stimulation in culture before being used for transfer experiments. All established T cell lines were  $\alpha\beta$ TCR<sup>+</sup>, CD4<sup>+</sup>, CD8<sup>-</sup> and displayed an effector memory phenotype (L-selectin<sup>-</sup>, CD45RC<sup>low</sup>, and CD44<sup>high</sup>). Upon stimulation, they produced IFN $\gamma$  and IL17. Phenotype, cytokine profile, antigen specificity, pathogenicity and the absence of mycoplasma contamination were verified in each cell line.

## **EAE models, and scoring system**

### ***Adoptive Transfer EAE and T cell mediated grey matter disease***

Fully activated T<sub>MBP</sub> or T<sub>bsYN</sub> cell blasts (D2 after antigen encounter) were injected in the tail vein of recipient wt animals in EH medium. If not stated otherwise,  $2.5 \times 10^5$  T<sub>MBP</sub> cell blasts or  $1.5 \times 10^6$  T<sub>bsYN</sub> cell blasts per animal were transferred. As control,  $2.5 \times 10^5$  T<sub>OVA cells</sub> cells were i.v. injected following the same procedure.

### ***Lung EAE***

Resting T<sub>MBP</sub> cells ( $7.5 \times 10^6$ , D6 after antigen encounter) in EH medium were injected into the tail vein of recipient wt animals. Six hours later the animals were immunized intratracheally (i.tr.). For this purpose, rats were shortly anesthetized with ether and fixed with a bar behind their upper incisors on a stand in an upright position slightly leaning backwards. The trachea was located using a Small Animal Laryngoscope LS-2 (Penn Century). Subsequently, an emulsion consisting to equal parts of antigen, i.e. MBP or OVA (0.02 mg/mL), and CFA (0.2 mg/mL) was instilled into the trachea through a winged 18G catheter (B. Braun). Each animal received a total volume (in µL) corresponding to around one-third of its body weight (in g). The

animals were then released from the stand and transferred to their cages to recover. The entire procedure typically lasted approximately 1 min per animal.

### ***Subcutaneous EAE***

Resting T<sub>MBP</sub> cells ( $7.5 \times 10^6$ , D6 after antigen encounter) in EH medium were injected into the tail vein of recipient wt animals. Six hours later an emulsion consisting to equal parts of antigen, i.e. MBP or OVA (1 mg/mL), and CFA (1 mg/mL) was injected subcutaneously (s.c.) into the popliteal cavities of both hind limbs of ether-anesthetized animals. Each animal received a total volume (in  $\mu$ L) corresponding to around one-third of its body weight (in g).

### ***EAE scoring***

Weight and clinical scores were recorded daily. Classical signs of EAE were scored as follows: 0 = no disease; 1 = flaccid tail; 2 = gait disturbance; 3 = complete hind limb paralysis; 4 = tetraparesis; 5 = death. For atypical symptoms that could occur upon transfer of T<sub>BSYN</sub> cells, the following classification was used: 0 = no disease; 1 = occasional twitches and scratching with or without flaccid tail; 2 = frequent twitches and scratching, ataxia; 3 = severe tonic and myoclonic movements, severe gait impairment; 4 = tetraparesis; 5 = death. Animals with a clinical score above 3 were sacrificed.

No statistical method was used to predetermine sample size. Clinical score was assessed in a blinded fashion. Animals were randomly allocated to experimental groups.

### ***Antibiotic treatment***

Neomycin (NEO; Thermo Fisher Scientific) or vancomycin (VANCO; Abcam) were administered i.tr. (daily dose: 0.1 or 1 mg; volume: 150  $\mu$ L), s.c. into the popliteal cavity (daily dose: 1 mg; volume: 50  $\mu$ L) or orally by gavage (daily dose: 1 or 10 mg; volume: 300  $\mu$ L). The i.tr. dose of antibiotics was selected upon initial titration on the basis that it did not change the

immune cell composition of the lung. Polymyxin B (Roth) was administered i.tr. (daily dose: 0.1 mg; volume: 150  $\mu$ L). The antibiotics were freshly prepared before every treatment by dissolving the powder in sterile PBS. An equivalent volume of PBS was used as control. If not stated otherwise, NEO and VANCO were administered at a daily dose of 1 mg/animal. The animals were treated daily for 7 days before starting the experiment. Daily treatment was continued throughout the entire experiment. Of note, both the i.tr. and oral antibiotic treatments were well tolerated by the animals. No respiratory distress or diarrhea were observed and the animals steadily increased their body weight comparably to the controls.

### **Transfer of BALF-derived microbiota**

Animals were i.tr. treated with NEO. After 7 days, the treatment was stopped and the animals were i.tr. transferred with BALF-derived microbiota of animals i.tr. pre-treated for 7 days with either PBS or NEO (Donor group). Immediately after the microbiota transfer, EAE was induced by i.v. injection of T<sub>MBP</sub> cells. The treatment with BALF derived microbiota was performed daily for the entire disease course.

For the collection of microbiota, sterile BALF (8 mL/animal) was collected daily either from the PBS- or the NEO-donor group as described below (see: Collection of BALF and fecal samples). The BALF was centrifuged for 10 min at 13.000 rpm and 4 °C and the bacterial pellet re-suspended in 450  $\mu$ L sterile PBS. Each animal of the recipient group received a daily dose of 150  $\mu$ L of the corresponding BALF re-suspension.

### **Functional inhibition of microglia by minocycline treatment**

PBS-treated or NEO-treated rats received i.p. minocycline-hydrochloride (Sigma-Aldrich) dissolved in 40 % 2-hydroxypropyl- $\beta$ -cyclodextrin (vehicle; ITW Reagents; daily dose: 50

mg/kg rat body weight). Injection of the same volume of vehicle served as control. Treatments with PBS/NEO and Minocycline/vehicle started 7 days before T<sub>MBP</sub> cell transfer and were continued throughout the entire EAE course. Of note, the i.p. treatment was well-tolerated by the animals. No distress was observed and the animals steadily increased their body weight comparably to the controls.

### **Depletion of microglia by PLX3397 treatment**

PBS-treated or NEO-treated rats received the CSF1R inhibitor PLX3397 (MedChemExpress) dissolved in 0.5% HPMC/1% Tween80 /2.5% DMSO (daily dose: 30 mg/kg rat body weight) or vehicle by gavage. Treatments with PBS/NEO and PLX3397/vehicle started 7 days before T<sub>MBP</sub> cell transfer and were continued throughout the entire EAE course. Of note, the per os (p.o.) treatment was well-tolerated by the animals. No distress was observed and the animals steadily increased their body weight comparably to the controls.

### **Treatments with poly I:C, inactivated *Prevotella melanogenica* and LPS**

#### *Poly I:C treatment*

Polyinosinic-polycytidylic acid sodium salt (poly I:C; Sigma-Aldrich) was dissolved in sterile water at a stock concentration of 10 mg/mL. Aliquots were stored at -20 °C and thawed shortly before injection. Poly I:C solution (1 mg in 100 µL) was administered i.th. in animals anesthetized with Ketamine (50 mg/kg, Medistar) and Xylazine (10 mg/kg Ecuphar). Half of the dose (50 µL) was injected into the cisterna magna, the remaining half into the lumbar spinal cord (L4-L5) using a stereotactic device (Narishige). The treatment was performed on D0, D2 and D4 after T<sub>MBP</sub> cell transfer. Sterile PBS was used as control. Of note, 24 h after i.th. injection, the animals displayed a reduction in body weight as reported<sup>47</sup>. As this symptom

occurred independently of EAE symptoms, body weight changes are not depicted in the corresponding graphs.

#### *Treatment with inactive Prevotella melaninogenica*

*Prevotella melaninogenica* (*P. melaninogenica*; type strain DSM 7089; DSMZ, Germany) was grown anaerobically in modified PYG medium (Medium 104; DSMZ, Germany) at 37 °C. For transfer experiments of inactive *P. melaninogenica*, the culture was grown to a concentration of  $30 \times 10^6$  CFU/mL. The culture was chemically inactivated using chicken egg lysozyme (2 mg/L; SERVA) and subsequently heat-inactivated at 99 °C for 30 min. Successful inactivation was verified by the inability of the bacteria to regrow in culture. Before transfer, the samples were centrifuged at 13,000 rpm for 10 min at 4 °C and re-suspended in sterile PBS. Animals received daily  $5 \times 10^5$  CFU in 150 µL sterile PBS daily or 150 µL sterile PBS as control either i.tr. or p.o. The treatment was started 7 days before disease induction by transfer of T<sub>MBP</sub> cells and continued through the entire experiment.

#### *P. melaninogenica LPS treatment*

For LPS extraction, *P. melaninogenica* was cultured as described above (see: Treatment with inactive inactive *Prevotella melaninogenica*). The culture was grown to an OD<sub>600</sub> of 0.8-1.2. LPS was extracted using a LPS Extraction Kit (iNtRON) according to the manufacturer's instructions. The yield was quantified using the Pierce™ Chromogenic Endotoxin Quant Kit (Thermo Scientific). *E. coli* LPS (serotype 0127: B8; Sigma-Aldrich) served as an additional control.

Solution with LPS from *P. melaninogenica* was freshly prepared before every treatment by dissolving the isolated LPS pellet in sterile PBS by boiling the vial for 5 min. *P. melaninogenica* LPS was administered i.tr. (dose: 0.01 or 0.025 mg in 150 µL PBS) or i.th. (dose: 0.005 mg in 30 µL PBS). For the i.tr. treatment, LPS was administered daily starting on D7 before disease induction by transfer of T<sub>MBP</sub> cells and continued through the entire experiment. For i.th.

treatment, *P. melaninogenica* LPS was injected as above in the cisterna magna on D0, D2 and D4 after  $T_{MBP}$  cell transfer. Sterile PBS was used as control.

#### *E. coli* LPS treatment

*Escherichia coli* (*E. coli*; serotype 0127: B8; Sigma-Aldrich) was administered i.tr. (0.01 mg in 150  $\mu$ L PBS) or i.th. (0.003 mg in 30  $\mu$ L PBS) following the same schedule as for *P. melaninogenica* LPS treatments. The daily i.tr. LPS dose was 50 times lower than the dose administered in a model of acute lung injury<sup>48</sup> and was well-tolerated by the animals. No respiratory distress was observed and the animals steadily increased their body weight comparably to the controls. Upon i.th. treatments with either *P. melaninogenica* or *E. coli* LPS, as observed upon poly I:C administration, the animals displayed a reduction in body weight not related to EAE. Therefore, body weight changes are not depicted in in the corresponding graphs.

### **Lung and gut microbiota analysis**

#### *Description of the samples*

For characterizing the changes of lung and gut microbiota upon i.tr. antibiotic treatment, bronchoalveolar lavage fluid (BALF) and faeces samples were collected from animals daily treated with NEO (0.1 or 1 mg/day), VANCO (0.1 or 1 mg/day) or PBS for 7 days. For each cohort, 6 samples from 2 independent experiments each including 3 animals/group/treatment were analyzed. For characterizing the changes in gut microbiota upon oral antibiotic treatment, faecal samples were collected from animals daily treated with NEO (1 or 10 mg/day) or PBS for 7 days. For each cohort, 6 samples from 2 independent experiments each including 3 animals/group/treatment were analyzed.

#### *Collection of BALF and fecal samples*

BALF and fecal samples were collected under sterile conditions from the same animals. Briefly, the rats were euthanized using an overdose of Ketamine/Xylazine. After carefully disinfecting the animal's fur with 70 % EtOH, a tracheotomy was performed and a sterile gavage needle (18G) inserted into the trachea under a laminar flow hood. The gavage needle was fixed and held in position using a surgical suture (B. Braun.). 5 mL pre-warmed (37 °C) PBS were slowly instilled into the lung and after 30 s a volume of 4 mL was retrieved. This step was repeated once, yielding 8 mL of total BALF per animals. Fecal samples were collected from the recto-anal region. BALF (in 2 mL aliquots) and fecal samples were immediately snap-frozen on dry ice and stored at -80 °C until further processing.

#### *Lysis and nucleic acid extraction*

To efficiently extract nucleic acids from both gram-positive and gram-negative bacteria, a pre-lysis step was performed by incubating 400 µL BALF with 2 µL chicken egg lysozyme (100 mg/mL; SERVA) at 37 °C and 180 rpm for 1 h. DNA extraction from BALF was performed using the QIAamp cadior Pathogen Mini Kit (Indical Bioscience) according to the manufacturer's instructions. DNA was eluted with 50 µL sterile water. Rat fecal samples (~150 mg) were re-suspended in 1 mL InhibitEX buffer (QIAGEN) at 37 °C for 15 min for homogenization and mixed every 5 min with an inoculation loop. Fecal sample DNA was extracted using the QIAamp Fast DNA Stool Mini Kit (QIAGEN) according to the manufacturer's instructions. DNA was eluted with 200 µL sterile water. Extracted nucleic acids were quality-checked via 0.8 % LE Agarose (Biozym) gel electrophoresis. Nucleic acid concentrations were quantified using a NanoDrop ND-1000 Spectrophotometer (Thermo Scientific).

#### *Quantification of bacterial number*

The bacterial load of rat BALF and fecal samples was estimated by analyzing the expression of the protein elongation factor Tu (*tuf*) gene by real-time quantitative PCR using the Bacteria (*tuf*

gene) quantitative PCR Kit (Takara) and an iQ<sup>TM</sup>5 Multicolor Real-Time PCR Detection System (BioRad). PCR and cycling conditions were set according to the manufacturer's instructions. All samples were prepared at least in duplicate. CT values of the individual measurements did not exceed 1.5 amplification cycles. For the BALF samples, the copy number of the *tuf* gene was normalized to 100  $\mu$ L for each sample. Fecal samples were normalized based on the weighed amount used for DNA extraction. The copy number of the *tuf* gene was finally normalized for 100  $\mu$ g of feces for each sample.

#### *16S amplicon generation and sequencing*

Bacterial 16S rRNA amplicons were generated using Klindworth primers with adapters for Illumina MiSeq sequencing targeting the V3 – V4 region<sup>49</sup>. For BALF samples polymerase chain reaction mixtures (50  $\mu$ L) contained 1x Phusion GC buffer (5x), 0.2 mM of each deoxynucleoside triphosphates, 5 % DMSO, 0.1 mM MgCl<sub>2</sub>, 0.2  $\mu$ M of each primer, 0.02 U of Phusion<sup>TM</sup> High-Fidelity DNA Polymerase (Thermo Fisher Scientific) were used. As template, approximately 150 or 350 ng of isolated BALF or fecal DNA, respectively was used. Negative and positive controls contained no DNA template or genomic *Bacillus* DNA, respectively. For amplicon amplification of BALF samples, the following cycler program was used: initial denaturation at 98 °C for 1 min, 35 cycles of denaturation at 98 °C for 45 s, annealing at 62 °C for 45 s and extension at 72 °C for 45 s, followed by a final extension at 72°C for 5 min. For fecal samples, the 25 PCR cycles were performed with an extension time of 30 s. Each PCR reaction was performed in triplicate. The resulting PCR products were pooled in equal amounts and purified with the MagSi-NGSPrep Plus Kit (Steinbrenner) according to the manufacturer's instructions. Amplicons were eluted in 40  $\mu$ L sterile water and quantified with the Quant-iT dsDNA HS assay kit and a Qubit fluorometer (Invitrogen). The indexing of the amplicons was performed with the Nextera XT Index-Kit (Illumina). 16S rRNA gene sequencing was

performed using the dual index paired end approach (2x 300 bp) with v3 chemistry for the Illumina MiSeq platform.

### *16S rRNA Sequence Data Processing*

Raw sequencing data were initially processed by using the Miseq marker gene pipeline v1.8<sup>50</sup>. Further processing was performed using VSEARCH v2.12.06<sup>51</sup> and UNOISE3 algorithm. Raw sequencing reads were mapped to the amplicon sequence variant (ASV) table. The similarity threshold was set at 100 %. Taxonomic classification of ASVs was performed using BLASTn 2.7.1 against the SILVA SSU NR database release 138<sup>52,53</sup>. If not otherwise stated, all bioinformatic tools were used with default parameters.

### *Statistical Analyses*

Subsampling, removal of chloroplasts, eukaryote, mitochondria, archaea and unclassified ASVs, as well as statistical analysis including diversity analysis and visualization was performed in Rstudio version 1.3.1056 (RStudio Team, 2020) and R 4.0 (R Core Team, 2013). Inter-sample data normalization was performed in R using the geometric mean of pairwise ratios package (GMRP v0.1.3)<sup>54</sup>. Data were visualized by using ampvis2 (v2.6.4)<sup>55</sup> and the implemented package ggplot2 (v3.3.2)<sup>56</sup>. Alpha-diversity metrics and species richness were used to characterize the bacterial diversity within each sample, which included calculation of the Shannon diversity index and phylogenetic diversity index. All samples were rarefied in ampvis2 to the corresponding lowest number of reads per treatment. The normality of data distribution was examined by the Shapiro–Wilk test. ANOVA was used to compare parametric variables among three or more groups, and the Kruskal–Wallis test was used for non-parametric variables. To compare means between unpaired groups with an assumption of unequal variance between sample sets the independent *t*-test was used and for non-parametric variables the Mann–Whitney U-test. *p*-values less than 0.05 were considered to indicate statistical significance. For visualization in bar charts, the mean of treatment replicates was used to

account for the variance in animal samples. To visualize the multivariate dispersion of the composition of the community non-metric multidimensional scaling (NMDS) matrix of the Bray-Curtis dissimilarity between samples was calculated by the *ampvis2* package (version 2.6.4) wrapping around the *vegan* package (version 2.5-6) using the ASV table and the phylogenetic tree. Ordination plots were created with *ggplot2* (3.3.2) with *bray* as distance measure. For heatmaps the *amp\_heat* function implemented in *ampvis2*<sup>55</sup> was used to identify the most abundant taxa (mean) in different treatments and antibiotic concentration. Taxonomic classification is indicated on class and genus level.

### **Quantitative analysis of LPS**

The amount of LPS in BALF samples was measured in triplicates using the Pierce Chromogenic Endotoxin Quant Kit (Thermo Fisher Scientific) according to the manufacturer's instructions. Values are expressed in international endotoxin units (EU)/mL.

### **Cell isolation**

Animals were intracardially perfused for 6 min with PBS before organ explant. Mononuclear cells were isolated as previously described<sup>2,10</sup> and kept on ice in EH medium until processed. The procedures are briefly summarized below: EDTA-treated blood was retrieved from the heart by cardiac puncture. Mononuclear cells were isolated by density gradient using Lymphocyte Separation Medium (*PromoCell*; centrifugation settings: 30 min at 840 x g and 20°). Lungs were thoroughly and repeatedly sectioned using a tissue chopper (McIlwain). The homogenized tissue was washed with EH. Pellets were re-suspended and incubated with 2 mL of 0.3 % collagenase in PBS for 30 min at 37 °C under constant shaking. Subsequently, the tissue was homogenized using a gentleMACS Dissociator (Miltenyi Biotec), forced through a

cell strainer (40  $\mu$ m) and washed with EH. The pellet was re-suspended in 5 mL 40 % isotonic percoll and underlayed with 5 mL 70 % percoll (centrifugation settings: 30 min at 2000 rpm and 4°). The leukocyte-enriched interphase was then collected, washed and re-suspended in EH medium. Spleens and lymph nodes were passed through a cell strainer (40  $\mu$ m), washed once with PBS and treated with ACK-buffer for erythrocyte lysis. Parenchyma and leptomeninges of brain and spinal cord were passed through a cell strainer (40  $\mu$ m) and washed once with PBS. Myelin debris was eliminated by Percoll-density gradient (centrifugation settings: 30 min at 700 x g and 4 °C). For endothelial cell isolation, spinal cords were dissected, and the meninges were removed from the parenchyma. Spinal cord parenchyma were brought to single cell suspension using a Dounce homogenizer. The meninges were chopped up using a razor blade. The CNS tissues were then digested with liberase (0.4 U/mL; Roche) and DNase I (120 U/mL; Roche) at 37 °C for 1 h with gentle pipetting of the solution every 10 min. Subsequently, the cell suspension was passed through a 40  $\mu$ m cell strainer. Myelin debris was removed using a Percoll-density gradient as described above. After washing, the pellets were antibody-labelled in staining-buffer and FACS-sorted as described below.

### **Flow cytometry and fluorescence-activated cell sorting**

Flow cytometry analysis was performed with a FACSCalibur operated by Cell Quest software (Becton Dickinson) or with a CytoFLEX flow cytometer (Beckmann Coulter).

The following anti-rat mAbs were used for surface staining:  $\alpha\beta$ TCR-AF647 (clone R73, Biolegend), CD45RA-PE (clone OX-33; Biolegend), CD8 $\alpha$ -FITC (OX-8; Biolegend) and CD8 $\alpha$ -PerCP (BD Biosciences), CD4-PE/Cy7 and CD4-PE/Cy5 (Clone W3/25; both BD Biosciences), CD134-BV421 (Clone OX40, BD Biosciences), CD25-PE (Clone OX39 Biolegend), CD62L-PE (clone OX85, Biolegend), LFA-1-APC (integrin  $\alpha$ L, clone WT.1, Serotec), VLA-4-APC (anti-CD49d, clone TA-2, Sigma-Aldrich), CD31-PE (clone TLD-3A12,

BD Biosciences), CD11b/c-PE and CD11b/c APC (clone OX-42, Biolegend), CD45-PE, CD45-AF647 and CD45-PerCP (clone OX-1; all Biolegend), GLAST-APC (ACSA1, Miltenyi), RT1B-FITC (clone OX-6, BD Biosciences), RP3-BV421 (BD Biosciences), CD172a-FITC (Clone ED9, Bio-Rad). Matching directly labelled mouse IgM (clone R6-60.2, BD Biosciences), mouse IgG-APC (Jackson) and Mouse IgG1 $\kappa$  (MOPC 31C, Sigma-Aldrich) were used as isotype controls. Antibodies were used at a concentration of 1:200.

For measuring IFN $\gamma$  and IL17 expression, *ex vivo* isolated cells were left unstimulated or stimulated *in vitro* with 1  $\mu$ g/mL PMA (Phorbol 12-myriyate 13-acetate, Sigma-Aldrich) and 5  $\mu$ M Ionomycin calcium salt (Sigma-Aldrich) for 30 minutes. Brefeldin A (5  $\mu$ g/mL) was added to block cytokine secretion. Cells were cultured for further 2 h and surface-stained with anti-rat  $\alpha\beta$ TCR-AlexaFluor647 (Clone R73, Biolegend), anti-rat CD4-PE/Cy7 (Clone W3/25, Biolegend) and anti-CD8 $\alpha$ -PerCP (Clone OX-8, Biolegend) for 30 minutes at 4° C. The cells were fixed with 2 % PFA, permeabilized with BD Perm/Wash buffer (BD Biosciences) and stained with rat anti-mouse anti-IL17-BV42 (clone TC11-8H4, Biolegend) and mouse anti-rat IFN $\gamma$ -PE (Clone DB1, Biolegend) for 45 minutes at 4°C. For intracellular staining for FoxP3 detection, *ex vivo* isolated cells were surface-stained as described above, fixed and permeabilized using FoxP3/transcription factors staining buffer set (eBioscience) following the manufacturer's instructions and stained with anti-mouse/rat/human FoxP3-PE (Biolegend).

For characterization of the expression profile, cells were sorted using a FACS Aria 4L SORP cell sorter (Becton Dickinson) controlled by FACS Diva software (BD) at a low flow rate under constant cooling (4 °C). T<sub>MBP</sub> cells, endogenous  $\alpha\beta$ TCR<sup>+</sup> CD4<sup>+</sup> and CD8<sup>+</sup> T cells, CD45<sup>-</sup> CD11b<sup>-</sup>stromal cells, CD45<sup>+</sup> CD11b<sup>+</sup> ED9<sup>-</sup> interstitial macrophages, CD45<sup>+</sup> CD11b<sup>+</sup> ED9<sup>+</sup> alveolar macrophages/recruited monocytes and RP3<sup>+</sup> neutrophils were sorted from the lung. For obtaining T cells from lungs for transcriptome analysis, CD11b<sup>+</sup> cells were depleted prior to sorting using anti-PE MicroBeads for MACS separation (Miltenyi Biotec) according to the

manufacturer's instructions. For characterization of CNS resident cells in NEO- vs. PBS-treated animals, CD11b<sup>-</sup> GLAST<sup>+</sup> astrocytes and CD45<sup>low</sup> CD11b<sup>+</sup> microglial cells were sorted. In inflamed conditions, cell characterization was performed on CD45<sup>low</sup> CD11b<sup>+</sup> microglial cells and CD45<sup>high</sup> CD11b<sup>+</sup> MΦ, which comprise both recruited monocytes and resident macrophages. Of note, even though microglia upregulated CD11b in inflamed conditions, they were still well distinguishable from CD45<sup>high</sup> CD11b<sup>+</sup> MΦ (Extended Data Fig. 10). The sorted cells were centrifuged at 1500 x g for 4 min at 4 °C and the pellet was re-suspended in 300 μL TRI reagent (Merck) and 1 μL glycogen (Roche). The samples were stored at -80 °C until further processing. Data analysis was performed with FlowJo LLC (v10) or CytExpert (5.2) software.

Gating strategies used throughout the manuscript are depicted in Supplementary Figure 1.

### **Neomycin toxicity assay**

T<sub>MBP</sub> cells ( $5 \times 10^4$ /well) were challenged with MBP (10 mg/mL) in presence of irradiated thymocytes ( $5 \times 10^5$ /well) in 96-well flat bottom plates (Thermo Fisher Scientific). NEO was added in various concentrations (100 ng – 10 mg/mL). The cells were incubated at 37 °C and 10 % CO<sub>2</sub>. T cell proliferation was quantified by flow cytometry on D2, D3 and D4 after antigen encounter. On D2, 50 μL of IL2-containing growth medium were added to wells acquired on D3 (and 4). The same procedure was repeated on D3 for samples acquired on D4. In addition, following *in vitro* NEO exposure (1 or 10 mg/mL),  $2.5 \times 10^5$  T<sub>MBP</sub> cell blasts (D2 after stimulation) were adoptively transferred into naïve recipient rats and the clinical course of EAE was monitored over the following days.

### **Intravital TPLSM**

Two-photon laser-scanning microscopy (TPLSM) and spinal cord preparation were performed as described previously<sup>11,12,57</sup>. The procedures are briefly summarized below. TPLSM was used to image the motility and infiltration of fluorescently labelled T<sub>MBP</sub> and T<sub>OVA</sub> cells in the spinal cord of living rats. In addition, the technique was used to analyze BBB permeability. Imaging of T<sub>MBP</sub> cells was performed in the preclinical phase, at the onset and the peak of EAE.

### *Surgical procedures*

The animals were pre-anesthetized with a subcutaneous injection of 75 mg kg<sup>-1</sup> ketamine (Medistar) combined with 0.5 mg kg<sup>-1</sup> medetomidin (Vetpharm). Subsequently, they were intubated via a small incision of the trachea and immediately ventilated with 1.5 – 2% of isoflurane (CP-Pharma). During imaging, rats were stabilized in a custom-made microscope stage and their body temperature was regulated and maintained (36 – 37 °C) via a heated pad connected to a custom-built thermocontroller. Fluid supply during imaging sessions was maintained using a perfusing device (Ismatec) set to a 0.6 mL/h<sup>-1</sup> flow rate. Thoracic leptomeninges were accessed as described<sup>12,57</sup> by performing a laminectomy at level Th12/L1 and carefully removing the dura mater.

### *Technical equipment and labelling procedures*

TPLSM imaging was performed as previously described<sup>11,12,57</sup> using two different systems: (1) a Zeiss Laser Scanning Microscope 710 (Carl Zeiss) combined with a Coherent 10 W Ti:Sapphire chameleon laser (Coherent), controlled by Zeiss ZEN 2012 SP2 v2.1 software; and (2) an Olympus FVMPE-RS TPLSM equipped with a Spectra-Physics Mai Tai Ti:Sapphire oscillator and a Mai Tai DeepSee Ti:Sapphire oscillator. The excitation wavelength was tuned to 880 nm or 1,010 nm and routed through a 20x water 1.0 NA immersion objective W Plan Apochromat (Carl Zeiss) or a 25x water 1.05 NA immersion objective Olympus Scaleview. Excitation at 1,100 nm was propagated by either using a Ti:Sapphire laser pumped OPO in the Zeiss TPLSM or a Mai Tai DeepSee Ti:Sapphire oscillator in the Olympus TPLSM. Emitted

fluorescence was detected using non-descanned detectors equipped with 442/46 nm, 483/32 nm and 624/40 nm band-pass filters. Typically, areas of 424.27  $\mu\text{m}$  x 424.27  $\mu\text{m}$  (Zeiss) or 508.93  $\mu\text{m}$  x 508.93  $\mu\text{m}$  (512 x 512 pixels, Olympus) width were scanned and 50 – 100- $\mu\text{m}$  z-stacks were acquired. For overviews, several tile scans were acquired sequentially and stitched together. For reproducible motility analyses, the interval time was kept at 30 s for the Zeiss TPLSM and 15 s for the Olympus TPLSM, with a total acquisition time of 30 min per video. During motility experiments, the blood vessels were labeled with 70 kDa dextran Texas Red (Invitrogen) which was i.v. injected before the imaging session. For evaluation of the BBB permeability, 3 kDa dextran Texas Red (Molecular Probes) was i.v. injected during the imaging session (T=0).

#### *Analysis of time-lapse videos and statistics*

Acquired 3D time-lapse videos were analysed using Imaris 9.3.1 software (Bitplane AG). Cells were tracked using the automated Imaris Track module with subsequent manual revision. Motility parameters i.e. track length, track duration, track speed, track displacement and track straightness (ratio between total T cell path length and the sum of the entire single displacements) were calculated as described<sup>12,57</sup> within a 30 min recording interval. Rolling T cells were defined as cells appearing as single or several round-shaped dots with >50  $\mu\text{m}/\text{min}$  instantaneous velocity.

#### **RNA isolation, cDNA synthesis and quantitative real-time PCR**

Gene expression on transcription level was determined using quantitative real-time PCR. RNA was extracted from TRI Reagent (Merck) according to the manufacturer's instructions. Reverse transcription into cDNA was performed using the RevertAid First Strand cDNA synthesis kit (Thermo Fisher Scientific) according to the manufacturer's instructions. qPCR was performed on an Applied Biosystems StepOnePlus Real-Time PCR system (Thermo Fisher Scientific)

using custom-designed target-specific TaqMan probes quenched with TAMRA and labeled with FAM (Sigma-Aldrich).  $\beta$ -actin served as housekeeping gene. All measurements were performed in duplicate. The difference in the CT values between the individual measurements did not exceed 0.5 amplification cycles. The combinations of primers and probes used to detect  $\beta$ -actin, integrins, cytokines, chemokines, chemokine receptors, cyclins and egression factors have previously been described<sup>12,17,57</sup>. To detect the expression of tight junction genes, adhesion molecules, type I IFN-regulated genes and M2 macrophages markers the following combinations of primers and FAM-5'-3'-TAMRA probes were designed and tested:

*Vcam1*: Forward: ACATGAGGGTGCTCC TGTGA; Reverse: GGTGGCATTTCCTCGA GAGGA; Probe: TGTGCCAGCGAGGGT CTACCAGCTCCT. *Icam*: Forward: GGAGACAGCAGACCACTGTGCTT; Reverse: CTCGCTCTGGGAACG AATACA; Probe: ACTGTGGCACCACGC. *Cldn5*: Forward: CGGGCGTCCAGAGTTCAGT; Reverse: GTCGACTCTTTCCGC ATAGTCA; Probe: CCAGTCAAGTACTCA GCACCAAGGCGA. *Ocln*: Forward: CCTAATGTGGAAGAG TGGGTAAAAA; Reverse: GTCGACTCTTTCCGC ATAGTCA; Probe: CACACAAGACATGCCTCCACCCCC. *Mx1*: Forward: TCAA TTCAG AGTTCTTCTCGAGGAT; Reverse: GGGAG GTGAGC TCCATGGT; Probe: CCACAGTGCCCTGCTTGGCAA. *Mx2*: Forward: GAAATCTTCCA GCATCTGAATGC; Reverse: AAATACTGGATGATC AATGGAATGTG; Probe: TACCGCCAGGAGGCTCACAACCTGC. *Rsad2*: Forward: TTCCACACGGCCAAGACA; Reverse: ATACCAGCCTGTTTGAGCAGAAG; Probe: CCTTCGTGCTGCCCCTGGAGG; *Irf 8*: TGGTGACTGGGTATACTGCCTATG; Reverse: TGCCCCCGTAGTAAAAGTTGA; Probe: CGCACACCATTTCAGCCTTATCCCAG; *Irf7*: Forward: ACTTAGCCCCGGAGCT TGGAT; Reverse: GCACTGCTGAGGGTCACTTCT; Probe: TACAACCTGGCCC AGCTCTGGAGAACAG. *Oas1a*: Forward: GCGTCT GACTTGCCCTTGAG; Reverse: CGAGATACTGTCCACCCAGTGA; Probe: CCTTTGCCTGAGGAGCCACCCTTC. *Rtl-Ba*: Forward: GGTTGAGAACAGCAAGCCAGTC; Reverse: GGTGAGGTAAGCCATCTT GTGG; Probe: TGAGACCAGCTTCCTTTCCAACCCTGA. *B2M*: Forward: TCAGAAAACCTCCCCAAATTCAAG; Reverse: GACACGTA GCAGTTGAGGAAGTTG; Probe: ACTCTCGCCATCCACCGGAGAATG. *Il6st*: Forward: ATCAATTTTGACCCCGT GGAT; Reverse: TGGATAATTCTTCTGAGTTGGTCACT; Probe: AAGTGAAA CCCAGCCCACCTCATAATTTGT. *Arg1*: Forward:

GAAAGTCCCAGATGTACCAGGAT; Reverse: AGCCGATGTACACGATGTCCTT;  
Probe: CTGGGTGACCCCCTGCATATCTGC; *Mrc1*: Forward:  
CTGCAAAAAATCAGACGAAATCC; Reverse: TGTAGTAACAGTGGCCGTGGAA;  
Probe: TACGGAACCCCCACAGCTGCCTG. *Mrc1*: Forward: CTGCAAAAAATCAGA  
CGAAATCC; Reverse: TGTAGTAACAGTGGCCGTGGAA; Probe: TACGGAACCCCC  
ACAGCTGCCTG. *Ifnb1*: Forward: GCGTTCCTGCTGTGCTTCTC; Reverse:  
TGCTAGTGCTTTGTTCGGAAGT; Probe: CACTGCCCTCTCCATCGACTACAAGCAG.

### **RNA extraction, cDNA library preparation, and RNA-seq**

RNA extraction, cDNA library preparation, and RNA sequencing was performed as described<sup>11,57,58</sup> at the Transcriptome and Genome Analysis Laboratory (TAL) of the University Medical Center Göttingen. For T cell sequencing, total RNA was isolated from T<sub>MBP</sub> cells retrieved from the lungs of NEO- or PBS-treated animals on D0 and D1 post i.tr. immunization. Three different biological replicates were prepared for each sample. For each replicate, around 20,000 T<sub>MBP</sub> cells sorted from 4 to 5 rats with a purity >98 % were pooled. To address changes in the CNS expression profile upon antibiotic treatments, total RNA from total spinal cord tissue or from spinal cord derived CD45<sup>low</sup> CD11b<sup>+</sup> microglial cells was isolated from animals i.tr. treated for 7 days with NEO (1 mg/day), VANCO (1 mg/day) or PBS. Three and five different biological replicates were prepared for total spinal cord and microglia samples, respectively. For each replicate, spinal cord samples of 4 – 5 rats were pooled. Between 20,000 and 40,000 cells were sorted from each pooled microglial sample with a purity > 98 %. Library preparation for RNA-seq was performed using the TruSeq RNA Sample Preparation Kit (Illumina) starting from at 300 ng of total RNA. Single read (45 bp) sequencing was conducted using a HiSeq 2000 (Illumina). Illumina BaseCaller software was used to transform fluorescence images into BCL files. Samples were demultiplexed to FASTQ files with CASAVA. FastQC software was used to check the sequencing quality. Sequences were aligned to the Ensembl reference genome of *Rattus norvegicus* allowing for 2 mismatches within 45 bases. Quantification of gene

expression was done with the feature Countsprogram (version 1.5.1). Samples were subjected to differential expression analysis with DESeq2<sup>59</sup> (version 1.14.1). Gene annotation was performed using *Rattus norvegicus* entries from Ensembl. For analysis of T<sub>M</sub>BP cells in the lung, genes with a minimum one fold change and false discovery rate (FDR)-adjusted P<0.05 were considered differentially expressed. For the analysis of sorted microglia and spinal cord, where low differences in expression level were expected, genes with a minimum 0.5 fold change and false discovery rate (FDR)-adjusted P<0.05 were considered differentially expressed. KEGG pathway and GO term enrichment analysis were performed using the Database for Annotation, Visualization and Integrated Discovery (DAVID)<sup>60</sup>.

### ***In vitro* activation of microglia**

Microglial cells were isolated from the spinal cords of PBS- or NEO-treated rats using a three-phase Percoll density gradient as described<sup>11,61</sup>. Briefly, the spinal cord parenchyma was passed through a cell strainer (40 µm) and washed once with PBS. Microglia were isolated from the 75 % / 50 % isotonic Percoll interphase and washed once with PBS. Microglia from at least 6 animals per group were pooled. 10.000 microglia per well were plated in flat bottom 96-well plates in 50 µL DMEM based-medium containing 1 % rat serum. Another 50 µL of the above medium containing different concentrations of recombinant rat IFN $\gamma$  were added to each well, resulting in final concentrations of 0, 1, 10 and 100 ng/mL IFN $\gamma$ . Before transfer, the microglia of each well were centrifuged at 1500 x g for 4 min at 4 °C and the pellet was re-suspended in 300 µL TRI reagent (Merck) and 1 µL glycogen (Roche). The samples were stored at -80 °C until further processing.

### ***In vivo* activation of microglia by intrathecal delivery of cytokines**

For T cell-independent activation of the microglia, animals were i.tr. treated with PBS or NEO. Seven days later, a cytokine mix (volume: 30  $\mu$ L) composed of IFN $\gamma$  (250 ng) and TNF $\alpha$  (250 ng) was injected in the cisterna magna of anesthetized animals. Animals were analysed 4 and 18 h after i.th. injection. The cytokines IFN $\gamma$  and TNF $\alpha$  were selected because of their essential role in triggering CNS autoimmunity in rats<sup>11,62</sup>. The final cytokine dose and the analysis time-points were chosen based on preliminary experiments (data not shown) in which the cytokines were titrated and their effect on the CNS measured at different time intervals after injection.

### **Histology and immunohistochemistry**

Animals underwent PBS or NEO treatment for 7 days prior to intracardial perfusion with cold saline solution (10 min) followed by a cold fixative containing 4 % PFA (15 min). Samples were post-fixed in the same fixative for 24 h and then equilibrated in a 30 % sucrose solution. Thereafter, brains and spinal cords were embedded in cryoprotectant and stored at -20 °C. Brains and spinal cords were cut into 50  $\mu$ m thick coronal sections (brain coordinates from bregma: -1.92 to -3.72, spinal cord: L1 to L6) using a cryostat (Leica) and stored in PBS at 4°C until further use.

The sections were permeabilized and washed in PBS containing 0.3% Triton X-100. The blocking was performed with serum (5 %) from the secondary antibody host(s) for 1.5 h at RT. Thereafter, the slices were incubated with the primary antibodies in blocking solution (5 %) for 48 h at 4 °C. This step was followed by an overnight incubation at 4 °C with the suitable fluorophore-conjugated secondary antibodies in blocking solution (3 %). The sections were then mounted on SuperFrostPlus Slides (ThermoFisher) with Fluoromount-G (Southern Biotech). For microglia analysis (brain and spinal cord), anti-Iba-1 (1:500; Rabbit; polyclonal;

Wako 019-19741) and Rhodamine Red<sup>TM</sup>-X (RRX) anti-rabbit (1:200; Donkey; polyclonal; Jackson 711-295-152) were used as first and secondary antibody, respectively.

Images were acquired with a Zeiss Laser Scanning Microscope 710 (Carl Zeiss) controlled by Zeiss ZEN 2012 SP2 v2.1 software (Carl Zeiss) equipped with UV-diode for DAPI, a 488 nm Argon laser, a 561 nm DPSS laser and a 633 nm HeNe laser. Lasers were routed through a 40x oil NA1.3 immersion objective Plan Aplanachromat objective (Carl Zeiss). Pinhole size was set to 50  $\mu$ m. A z-step size between 0.5 and 1  $\mu$ m was chosen for optimal z-resolution. Morphological analysis and three-dimensional reconstruction of microglia was performed using Imaris 8.0.1 software (Bitplane AG) as described<sup>11</sup>. Confocal z-stacks were smoothed with both Median and Gaussian filters. Single cells were rendered by first using the filament tool to reconstruct the processes and later the surface tool to render the cell body. The 3D rendered images served for the quantitative analysis of morphological parameters.

### **Statistical analysis**

Statistical analysis was performed using GraphPad Prism (V6 – 8; GraphPad, USA) and Microsoft Excel (2010 and 2016; Microsoft, USA). Unless indicated otherwise, data are represented as mean  $\pm$  SEM (standard error of the mean). The statistical significance is reported in the figures. The statistical tests underlying data analysis are stated in the corresponding figure legends. Briefly, Gaussian distribution of independent data sets was tested using a Kolmogorov-Smirnov test with Lilliefors' correction. For comparing two datasets statistical significance was determined via unpaired two-tailed *t*-test in case of Gaussian and Mann-Whitney test in case of non-Gaussian distribution. For comparing more than two datasets, statistical significance was determined via one-way ANOVA with Tukey's multiple comparisons test in case of Gaussian and Kruskal-Wallis test with Dunn's multiple comparisons test in case of non-Gaussian distribution. In the case of the number of animals per experiment not being sufficient to test for

normality, Gaussian distribution was assumed unless differently indicated. Significance levels were set as  $*p < 0.05$ ;  $**p < 0.01$ ;  $***p < 0.001$ .

- 46 Määttä, J. A., Coffey, E. T., Hermonen, J. A., Salmi, A. A. & Hinkkanen, A. E. Detection of myelin basic protein isoforms by organic concentration. *Biochem.Biophys.Res.Communic.* **238**, 498-502 (1997).
- 47 Murray, C. et al. Interdependent and independent roles of type I interferons and IL-6 in innate immune, neuroinflammatory and sickness behaviour responses to systemic poly I:C. *Brain Behav Immun* **48**, 274-286, doi:10.1016/j.bbi.2015.04.009 (2015).
- 48 Rittirsch, D. et al. Acute lung injury induced by lipopolysaccharide is independent of complement activation. *J Immunol* **180**, 7664-7672, doi:10.4049/jimmunol.180.11.7664 (2008).
- 49 Klindworth, A. et al. Evaluation of general 16S ribosomal RNA gene PCR primers for classical and next-generation sequencing-based diversity studies. *Nucleic Acids Res* **41**, e1, doi:10.1093/nar/gks808 (2013).
- 50 von Hoyningen-Huene, A. J. E. et al. Bacterial succession along a sediment porewater gradient at Lake Neusiedl in Austria. *Sci Data* **6**, 163, doi:10.1038/s41597-019-0172-9 (2019).
- 51 Rognes, T., Flouri, T., Nichols, B., Quince, C. & Mahé, F. VSEARCH: a versatile open source tool for metagenomics. *PeerJ* **4**, e2584, doi:10.7717/peerj.2584 (2016).
- 52 Yilmaz, P. et al. The SILVA and "All-species Living Tree Project (LTP)" taxonomic frameworks. *Nucleic Acids Res* **42**, D643-648, doi:10.1093/nar/gkt1209 (2014).
- 53 Quast, C. et al. The SILVA ribosomal RNA gene database project: improved data processing and web-based tools. *Nucleic Acids Res* **41**, D590-596, doi:10.1093/nar/gks1219 (2013).
- 54 Chen, L. et al. GMPR: A robust normalization method for zero-inflated count data with application to microbiome sequencing data. *PeerJ* **6**, e4600, doi:10.7717/peerj.4600 (2018).
- 55 Andersen, K. S., Kirkegaard, R. H., Karst, S. M. & Albertsen, M. ampvis2: an R package to analyse and visualise 16S rRNA amplicon data. *bioRxiv*, doi:https://doi.org/10.1101/299537 (2018).
- 56 Wickham, H. *ggplot2: elegant graphics for data analysis*. 1-260 (Springer International Publishing, 2016).
- 57 Schläger, C. et al. Effector T-cell trafficking between the leptomeninges and the cerebrospinal fluid. *Nature* **530**, 349-353 (2016).
- 58 Cabeza, R. et al. An RNA sequencing transcriptome analysis reveals novel insights into molecular aspects of the nitrate impact on the nodule activity of *Medicago truncatula*. *Plant Physiol* **164**, 400-411 (2014).
- 59 Love, M. I., Huber, W. & Anders, S. Moderated estimation of fold change and dispersion for RNA-seq data with DESeq2. *Genome Biol* **15**, 550, doi:10.1186/s13059-014-0550-8 (2014).
- 60 Huang, d. W., Sherman, B. T. & Lempicki, R. A. Systematic and integrative analysis of large gene lists using DAVID bioinformatics resources. *Nat.Protoc.* **4**, 44-57 (2009).
- 61 Doorn, K. J. et al. Brain region-specific gene expression profiles in freshly isolated rat microglia. *Front Cell Neurosci.* **9**, 84 (2015).
- 62 Klinkert, W. E. et al. TNF-alpha receptor fusion protein prevents experimental auto-immune encephalomyelitis and demyelination in Lewis rats: an overview. *J Neuroimmunol* **72**, 163-168, doi:10.1016/s0165-5728(96)00183-x (1997).

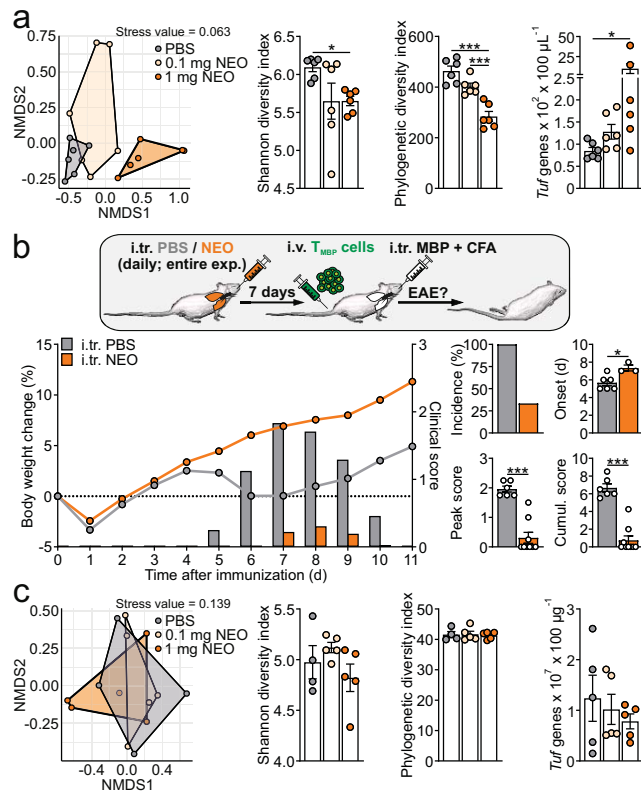
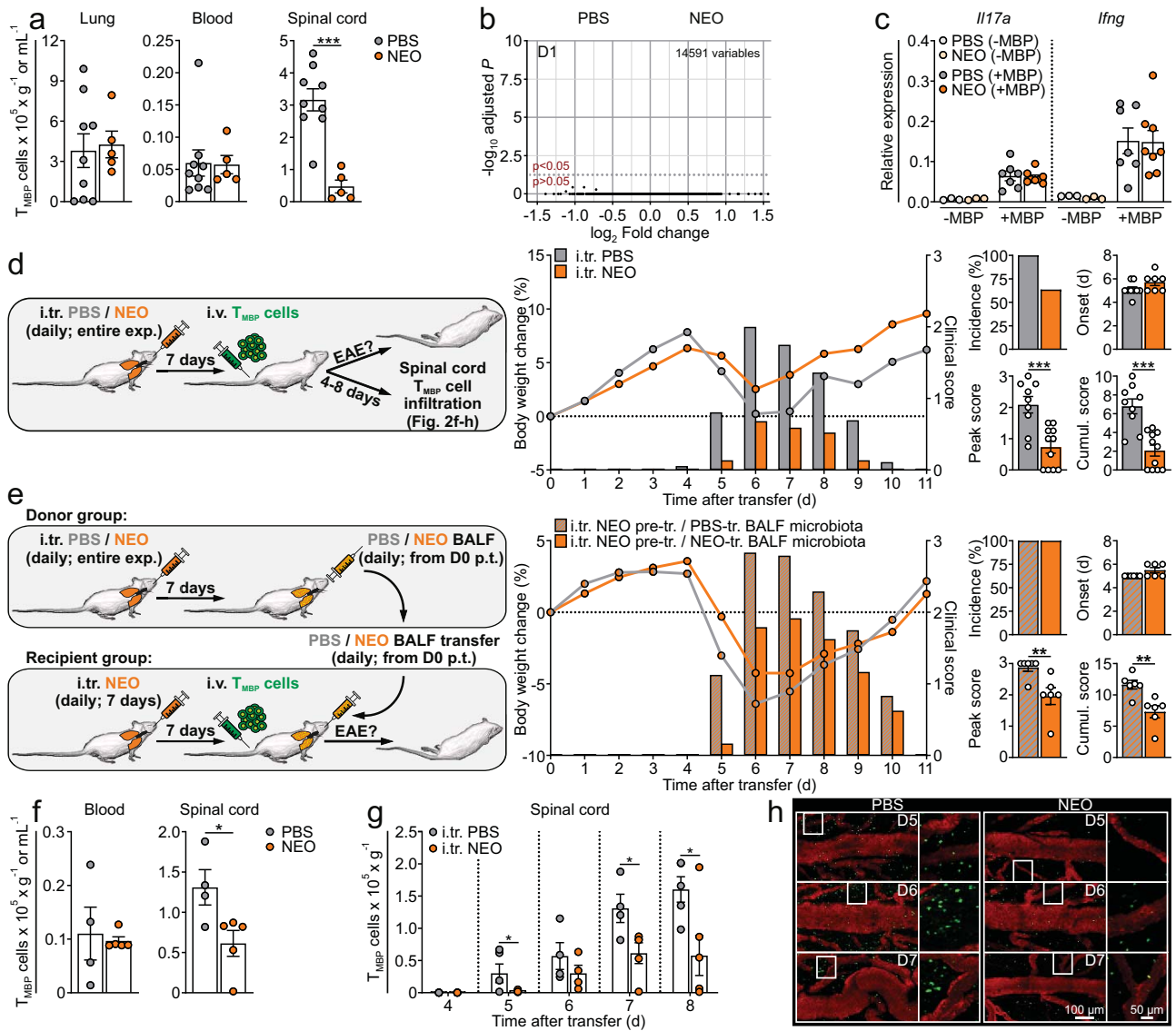
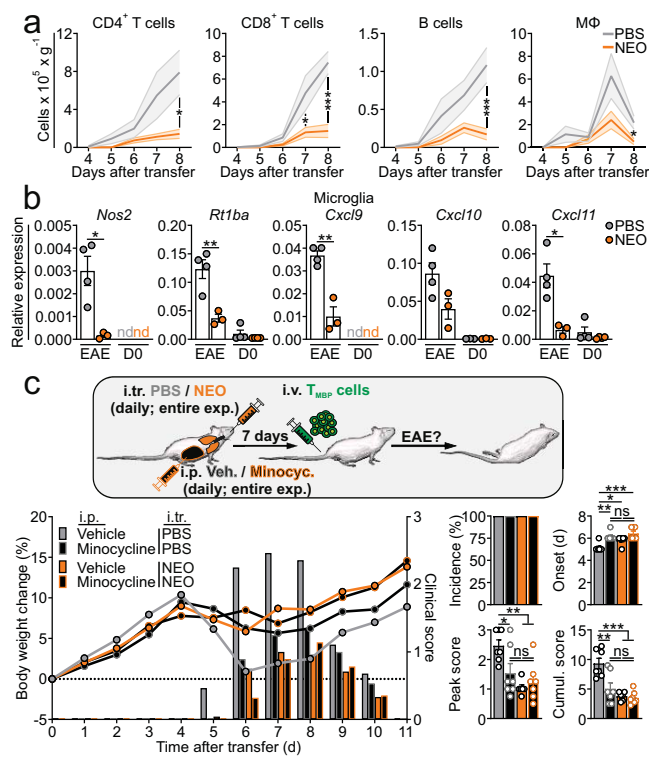


Fig. 1



**Fig. 2**



**Fig. 3**

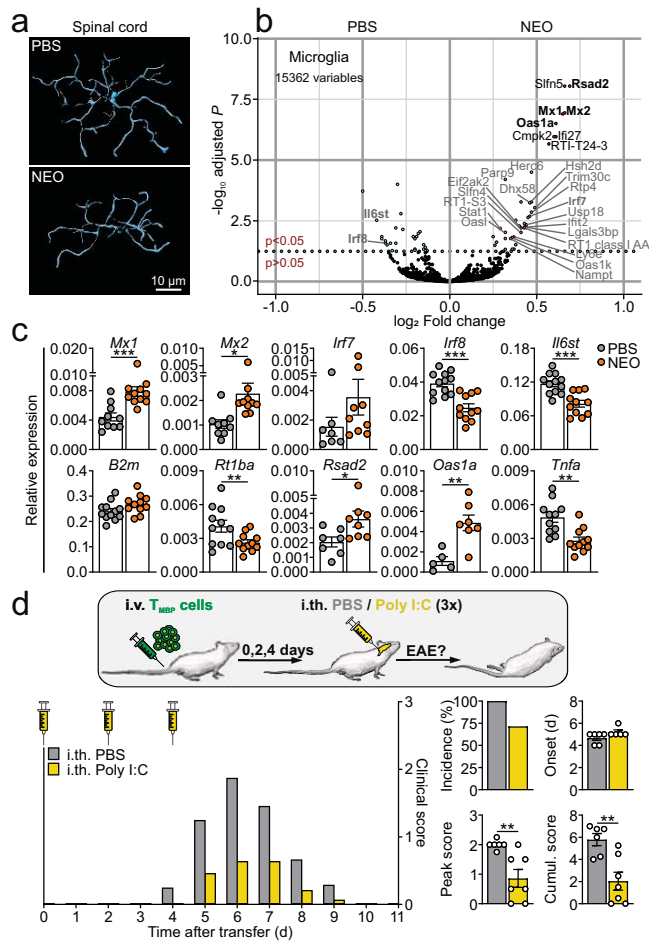


**Fig. 4**

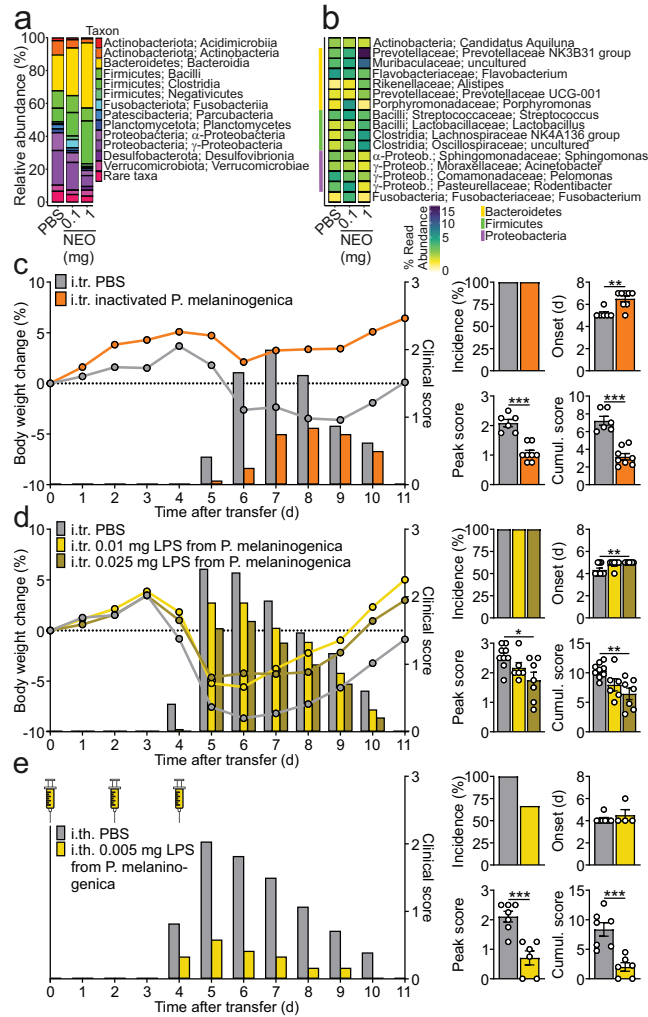


Fig. 5